Mon. Not. R. Astron. Soc. **000**, 1–21 (2012) Printed 4 March 2013 (MN LATEX style file v2.2)

# Near Infrared spectroscopy of post-starburst galaxies: a limited impact of TP-AGB stars on galaxy SEDs⋆

Stefano Zibetti[1,2]†, Anna Gallazzi[2], Stéphane Charlot[3], Daniele Pierini‡, Anna Pasquali[4]
[1] *INAF-Osservatorio Astrofisico di Arcetri - Largo Enrico Fermi, 5 - I-50125 Firenze, Italy*
[2] *Dark Cosmology Centre, Niels Bohr Institute - University of Copenhagen Juliane Maries Vej 30, DK-2100 Copenhagen, Denmark*
[3] *Institut dAstrophysique de Paris, CNRS, Université Pierre & Marie Curie, 98 bis Boulevard Arago, 75014 Paris, France*
[4] *Astronomisches Rechen-Institut, Zentrum für Astronomie der Universität Heidelberg, Mönchhofstrasse 12 - 14, 69120 Heidelberg, Germany*

arXiv:1205.4717v2 [astro-ph.CO] 3 Oct 2012

Accepted 2012 October 2. Received 2012 September 4; in original form 2012 May 20.

**ABSTRACT**

We present VLT-ISAAC near infrared (NIR) spectro-photometric observations of 16 post-starburst galaxies aimed at constraining the debated influence of TP-AGB stars on the spectral energy distribution (SED) of galaxies with stellar ages between 0.5 and 2 Gyr, hence critical for high-redshift studies. Post-starburst galaxies are characterised by negligible on-going star formation and a SED dominated by the stellar population formed in a recent ($< 2$ Gyr) burst. By selecting post-starburst galaxies with mean luminosity-weighted ages between 0.5 and 1.5 Gyr and a broad range of metallicities (based on SDSS optical spectroscopy), we explore the parameter space over which the relative energy output of TP-AGB stars peaks. A key feature of the present study is that we target galaxies at $z \approx 0.2$, so that two main spectral features of TP-AGB stars (C-molecule band-head drops at 1.41 and 1.77 $\mu$m, blended with strong telluric absorption features, hence hardly observable from the ground, for targets at $z \approx 0$) move inside the H and K atmospheric windows and can be constrained for the first time to high accuracy. Our observations provide key constraints to stellar population synthesis models. Our main results are: *i)* the NIR regions around 1.41 and 1.77 $\mu$m (rest-frame) are featureless for all galaxies in our sample over the whole range of relevant ages and metallicities at variance with the Maraston (2005) "TP-AGB heavy" models, which exhibit marked drops there; *ii)* no flux boosting is observed in the NIR. The optical-NIR SEDs of most of our post-starburst galaxies can be consistently reproduced with Bruzual & Charlot (2003) models, using either simple stellar populations (SSP) of corresponding light-weighted ages and metallicities, or a more realistic burst plus an underlying old population containing up to approximately 60% of the total stellar mass. In contrast, all combinations of this kind based on the Maraston (2005) models are unable to simultaneously reproduce the smoothness of the NIR spectra and the relatively blue optical-NIR colours in the observations. The data collected in this study appear to disfavour "TP-AGB heavy" models with respect to "TP-AGB light" ones.

**Key words:** galaxies: stellar content – stars: AGB and post-AGB – infrared: stars – infrared: galaxies – galaxies: general – galaxies: photometry

## 1 INTRODUCTION

The modelling of the spectral energy distribution (SED) of galaxies and its interpretation in terms of stellar population parameters (e.g. age, star formation history, metallicity) via stellar population synthesis (SPS) is a fundamental tool to understand the properties and evolution of galaxies. Yet, we are far from a complete comprehension and a reliable modelling of some stellar evolutionary phases which strongly affect the energy output of stellar populations. Among them, the so-called thermally pulsing - asymptotic giant branch (TP-AGB) phase has been the focus of debate among modellers for several years (e.g. Charlot & Bruzual 1991; Maraston 2005; Bruzual 2007; Marigo et al. 2008). This late stage of the AGB phase for low and intermediate mass stars ($M \lesssim 5$–$7$ M$_\odot$) culminates in stellar populations

⋆ Based on observations made with ESO telescopes at the La Silla Paranal Observatory under programme ID 086.B-0733.
† E-mail: zibetti@arcetri.astro.it
‡ Free-lance scientist

© 2012 RAS

of ages between 0.5 and 1.5 Gyr. TP-AGB stars emit mainly in the near infrared (NIR) spectral range given the low temperatures of these stars. Quantitative predictions of the lifetimes, luminosities and spectral shapes and features of these stars as well as of their impact on the integrated spectra of even "simple" stellar populations, are still very uncertain and strongly model-dependent (e.g. Melbourne et al. 2012). One further complication derives from the fact that TP-AGB stars are likely to be embedded in envelopes of dust produced by themselves (e.g. Groenewegen et al. 2009; Chisari & Kelson 2012), which attenuates the emerging optical and NIR radiation by a substantial fraction (Meidt et al. 2012).

The seminal work of Maraston (2005, Ma05 hereafter), who adopted the "fuel consumption theorem" approach and calibrated the flux contribution of this phase against optical and NIR photometry of Magellanic Clouds' globular clusters, dramatically pointed out how large the impact of TP-AGB stars on galaxy SEDs may possibly be. The Ma05 models make two clear and testable predictions in contrast to "classical" models (such as Bruzual & Charlot 2003, BC03 hereafter), which rely on standard, less extreme prescriptions for the TP-AGB phase: in particular, *i)* the NIR flux of stellar populations of ages between $\approx$0.5 and $\approx$ 1.5 Gyr is enhanced by a factor up to 3 (as a function of age and metallicity); in addition, *ii)* strong, sharp absorption features appear in the spectrum, especially at NIR wavelengths (and most notably at 1.1, 1.41 and 1.77 $\mu$m). These features correspond to the band-heads of carbon composite molecules and should depend on metallicity. They represent the undebatable fingerprints of TP-AGB stars as predicted by Ma05 models. This can be clearly seen in Fig. 1, where we confront the optical-NIR spectra of simple stellar populations (SSP) of three ages (0.5, 1 and 1.5 Gyr) at three different metallicities (0.5, 1 and 2–2.5 $Z_\odot$) as derived from the Ma05 models (black lines) and the BC03 models (red lines) respectively.

Observationally, detections of near-infrared CN absorption bands have been reported in the integrated spectra of only a few Seyfert galaxies (Riffel et al. 2007) and globular clusters dominated by the stochastic presence of bright carbon stars (Lyubenova et al. 2012). In fact, from a theoretical point of view, carbon absorption features are not a required signature of AGB-star populations. Sophisticated models of AGB stellar evolution predict that convective dredge-up of carbon produced by nuclear fusion during the envelope thermal pulses will increase the abundance of carbon relative to oxygen near the surface, which can eventually lead to the production of a carbon star (e.g. Marigo & Girardi 2007). While the efficiency of this process is expected to increase as the metallicity decreases, the integrated spectrum of most intermediate-age stellar populations could well be dominated oxygen-rich AGB stars without strong carbon absorption features.

The largely different NIR flux predictions for TP-AGB stars by different models have strong implications in terms of SED interpretation, leading to substantially lower stellar mass and age estimates (by up to a factor 2 or more) when rest-frame NIR bands are included in the analysis of galaxies with ages around 1 Gyr (e.g. Maraston 2005; Maraston et al. 2006; Kannappan & Gawiser 2007; Conroy et al. 2009; Ilbert et al. 2010). The popularity of NIR passbands as tracers of stellar mass, both at low and high redshift, thanks to their (generally) low sensitivity to age, metallicity and dust in terms of mass-to-light ratio (M/L) (e.g. Bell et al. 2003; Zibetti et al. 2009), clearly calls for a proper assessment of the models in this respect (see also Melbourne et al. 2012). Verifying the reliability of SPS models in the regime of ages around 1 Gyr is therefore of paramount relevance for studies of galaxy properties and their evolution.

Since 2005, a number of contrasting results and claims have been produced about the appropriateness of the Ma05 predictions. Maraston et al. (2006) showed that the Ma05 models fit the SEDs of high-z ($1.5 \lesssim z \lesssim 2.5$) galaxies better than BC03 models. However the same work shows that the performance of the two models differ only marginally in terms of goodness of fit if one allows for dust reddening, although the inferred stellar mass is substantially different. A better agreement of Ma05 models with the observed optical-NIR colours is also reported by MacArthur et al. (2010), who used combined optical spectroscopy and optical-NIR photometry to constrain the star formation history of two galaxies. Lyubenova et al. (2012) also report detections of the 1.77 $\mu$m feature in two Magellanic Clouds' globular clusters, in agreement with Ma05 predictions. On the other hand, studies of Magellanic Clouds' globular clusters found significant discrepancies between observations and Ma05 predictions. Lyubenova et al. (2010) found that the CO line strength (in the NIR K band) is much weaker than predicted by Ma05 in clusters of age $\approx$ 1 Gyr. Conroy & Gunn (2010) studied the colours of Magellanic Clouds' globular clusters as a function of their age and showed that Ma05 models predict optical and NIR colours that are too red. Moreover the predicted age dependence of these colours does not agree with the data. As opposed, a substantial agreement with models based on much less extreme TP-AGB prescriptions is found.

As already pointed out by Lançon et al. (1999), post-starburst galaxies (PSB hereafter) are the best galaxies to look at in order to find the fingerprints of (TP-)AGB stars on their SED. PSBs have a star formation history dominated by a burst in the exact age range when TP-AGB stars are expected to have the strongest impact, i.e. between 0.5 and 1.5 Gyr prior to the epoch of observation[1]. Their optical spectrum is characterised by a well developed Balmer/D4000 break, the lack of strong emission lines (which testify a substantial cessation of star formation activity) and by the very strong Balmer absorption lines typical of A stars (hence the alternative denomination of E+A or K+A galaxies). Conroy & Gunn (2010) compared the optical-NIR colours of the sample of PSBs spectroscopically selected by Quintero et al. (2004) to the colours of different SPS models. They showed (see their Fig. 16) that $i-z$, $g-r$ colours are not reproduced by Ma05 models: not only would the blue portion of this colour plane be only explained by unrealistically low metallicities, but also the age sequences in Ma05 models produce trends that are orthogonal to the observed age trends. Kriek et al. (2010) performed another photometric test, in which they fitted the stacked (rest-frame) UV-optical-NIR SED of 62 PSBs at $0.7 \lesssim z \lesssim 2$, colour selected

[1] This holds for several different star formation histories (see figs. 11 and 12 in Melbourne et al. 2012).

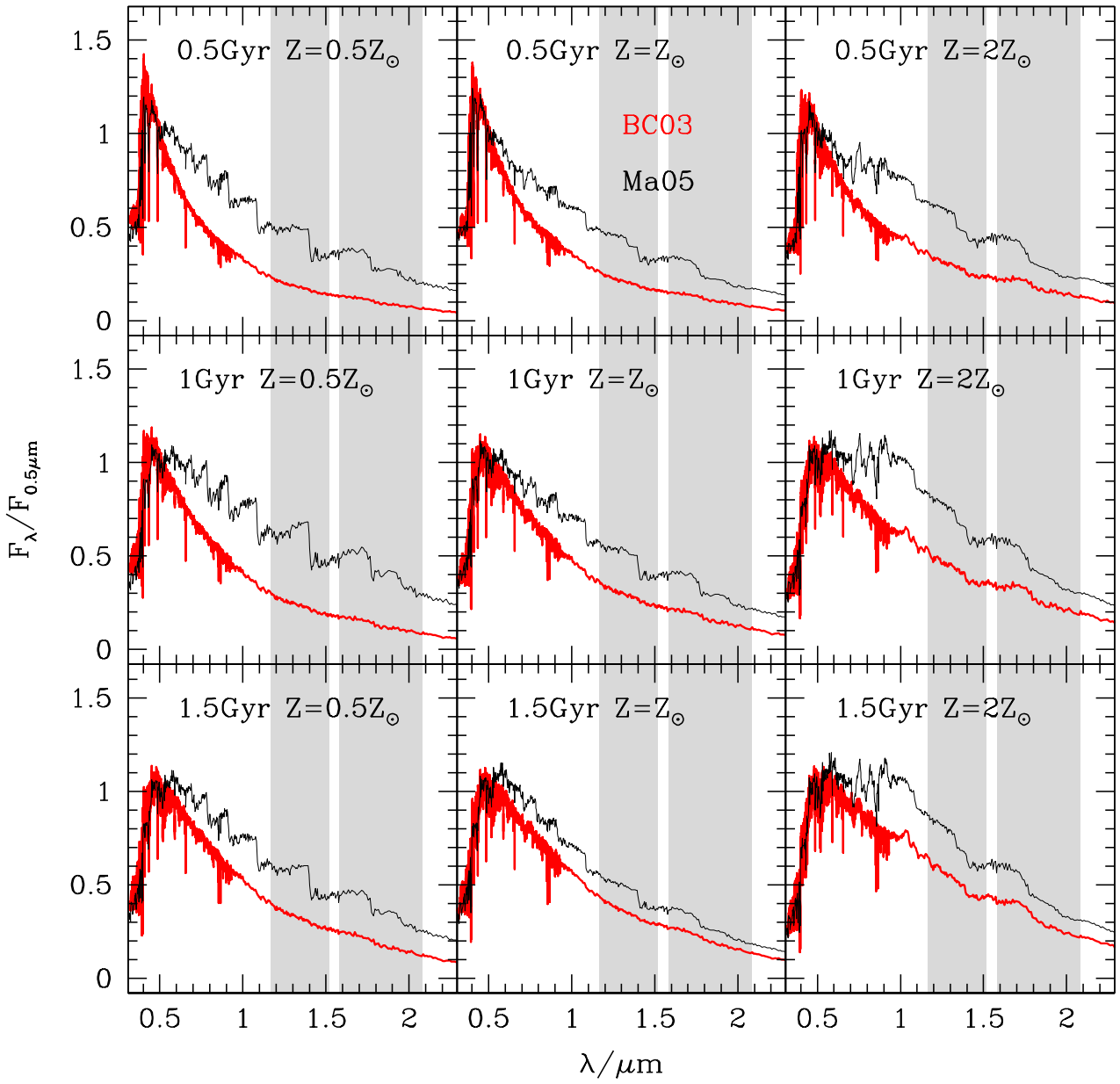


**Figure 1.** Comparison between SSPs at the peak of the TP-AGB phase, as derived from Ma05 models (black lines) and BC03 (red lines). Three different ages, 0.5, 1 and 1.5 Gyr from top to bottom, and three different metallicities, 0.5, 1 and 2 $Z_\odot$ (the highest metallicity for BC03 is actually replaced by 2.5 $Z_\odot$), from left to right, are considered. Shaded regions correspond to the rest-frame spectral ranges covered by the H and K band ISAAC spectroscopic setups for the $z \approx 0.2$ galaxies presented in this work and include the strong features at 1.41 and 1.77 $\mu$m.

from the *NEWFIRM* medium band survey (NMBS) to have ages around 1 Gyr, according to both BC03 and Ma05 models. Also in this case it is found that BC03 models can reproduce the observed SEDs much better, in particular the observed blue optical-NIR colours, which are not reproduced by Ma05.

In this paper we present the results of the experiment that we designed to test for the two main predictions of Ma05 models, namely the presence of sharp NIR spectral features and the boosted NIR flux, on a sample of PSBs carefully selected from optical spectroscopy and newly observed in NIR spectroscopy (H and K band) with ISAAC at the ESO-VLT. The selection criteria and properties of the sample are fully detailed in Section 2. Here we would like to stress the uniqueness of this work. *i)* For the first time we cover both the optical and the NIR range of PSBs with flux calibrated spectra to look directly for the NIR spectral features at 1.41 and 1.77 $\mu$m predicted by the Ma05 mod-

els and resulting from the large impact of TP-AGB C-rich stars. These features are unaccessible or extremely difficult to measure from the ground as they roughly coincide with the atmospheric gaps between J and H, and between H and K bands, respectively, for nearby objects. Therefore we observed PSBs in the redshift range 0.15–0.25 so that the C-features move well into the observable windows and are minimally affected by uncertain telluric corrections, as shown in Fig. 1. *ii)* Contrary to previous works based either on colour selection (Kriek et al. 2010) or on a purely phenomenological spectroscopic selection (Conroy & Gunn 2010), the selection of our sample is based on both phenomenological criteria (high Balmer line strength and low emission lines, Goto 2005) and bayesian estimates of light weighted ages from optical spectral indices as in Gallazzi et al. (2005). This allows us to focus our observations and analysis on the *precise* range of stellar ages where TP-AGB stars are expected to contribute the most, for a variety of stellar metallicities.

The paper is organised as follows. In Section 2 we present the sample, the new ISAAC NIR spectroscopic observations and the data reduction, including spectrophotometric calibrations and integration with optical data. In Section 3 we present the results and discuss possible spurious effects and contaminations that might affect our conclusions. A comparison with the analysis of Kriek et al. (2010) is also presented. Finally, in Section 4 we summarise our findings and propose our conclusions and future developments.

## 2 SAMPLE AND OBSERVATIONS

### 2.1 Sample selection and characterisation

We draw our PSB targets from the spectroscopic sample of the Sloan Digital Sky Survey (SDSS, York et al. 2000; Strauss et al. 2002) data release 7 (DR7, Abazajian et al. 2009). The initial pre-selection was based on the line equivalent width (EW) criteria defined in Goto (2005), namely: EW(H$\delta$)$>$ 5 Å, EW(H$\alpha$)$>$ $-3$ Å, EW([O II])$>$ $-2.5$ Å.[2] In order to ensure that the two strong NIR features corresponding to the band-heads of CN (1.41 $\mu$m) and $C_2$ (1.77 $\mu$m) due to carbon rich AGB stars (cf. Lançon & Mouhcine 2002) are observable from the ground, we require the galaxies to be at $0.15 < z < 0.25$, so that 1.41 $\mu$m and 1.77 $\mu$m (at rest) move into the H- and K-band windows, respectively. This selection is based on the SDSS-DR7 casjobs catalog[3]. We further restrict the sample by applying the visibility cuts in order for targets to be observable from Paranal during the winter semester: DEC$<$ 20 deg and RA between 0 and 230 deg or RA$>$ 330 deg. Finally we require that the stellar light-weighted age of the galaxies is in the range 0.5 to 1.5 Gyr, i.e. at the maximum of the predicted TP-AGB luminosity contribution, based on the estimates computed as in Gallazzi et al. (2005) and available in the MPA-JHU catalog[4]. Given the relative rarity of the post starburst phase and the restrictive age, coordinate and redshift cuts (the latter particularly relevant as it is almost at the extreme boundary of the SDSS main galaxy sample), the final sample is composed of sixteen galaxies only.

The properties of the sample are summarised in Table 1 and in Fig. 2. This figure illustrates the distribution of our galaxies in the classical H$\delta_A$ vs D4000$_n$ plane. In this plane the main sequence of galaxies with smooth continuum star formation history is displayed by the grey intensity levels, which represent the distribution of SDSS-DR4 galaxies of increasing ages from top-left to bottom right. Galaxies lying above this sequence, such as our galaxies, represented by the red dots with error bars, are characterised by relatively recent bursts of star formation with ages between a few hundred Myr to a couple of Gyr, which dominate the light of the galaxy. For comparison, tracks of Simple Stellar Populations (SSP) with different metallicities from BC03 are shown; the typical bell-shape of these SSP tracks peaks in H$\delta_A$ at ages of 0.3–0.5 Gyr (depending on metallicity) and decreases to H$\delta_A \approx$ 3–5 for ages of a few Gyr. By design, our sample populates the intermediate range of burst ages in this diagram.

The statistical estimates of light-weighted stellar ages, metallicity and mass computed from optical spectral absorption indices (D4000$_n$, H$\delta_A$ + H$\gamma_A$, H$\beta$, [MgFe]$'$, [$Mg_2$Fe]) with the bayesian method of Gallazzi et al. (2005) and used in the selection are reported in Tab. 1 (columns 6, 7 and 8), along with the ID (1), coordinates (2, 3), redshift (4) and apparent $r$-band petrosian magnitudes (5) of the galaxies from the SDSS. The sample comprises intermediate mass galaxies, between $\approx 3$ and $\approx 7 \times 10^{10} M_\odot$, with ages in the range $0.8 - 1.4$ Gyr and metallicities between 0.2 and 2.3 solar. Most galaxies have indeed $Z > 0.5 Z_\odot$, as expected given their stellar mass. Despite the paucity of galaxies at low age ($<$ 1 Gyr) *and* low metallicity ($< 1 Z_\odot$), the sample provides a good coverage of the relevant ages for the TP-AGB phase and of the metallicities most typical for galaxies around the characteristic luminosity $L^*$.

We note that the estimates of the stellar population parameters of Gallazzi et al. (2005) rely on the comparison with synthetic spectral libraries based on BC03 models, therefore they could be biased with respect to estimates based on other synthesis models, most notably the Ma05 ones. However, optical spectral indices short-wards of 5500 Å are generally well agreed upon among different modellers and, most importantly, are only weakly affected by TP-AGB stars, which mainly influence the NIR spectral region. Thus age and metallicity estimates from optical absorption features are robust against different TP-AGB prescriptions and the use of different models. This is even more the case for spectra dominated by A stars, where Balmer absorptions are very strong. Furthermore, in Sec. 3 (3.2 and 3.3 in particular) we thoroughly explore if and how different (combinations of) ages and metallicities can possibly explain the observed properties of our galaxies, irrespective of their original selection.

Based on the SDSS optical images and, to minor extent, on our ISAAC NIR images, we note that the majority of galaxies display smooth and centrally concentrated light distributions, typical of early type galaxies, with the only exception of PSB J0227−0015, which has an extended and irregular "halo". However, other four galax-

[2] We adopt the convention of positive EW for absorption and negative EW for emission. For the [O II] emission, the sum of the doublet is considered.

[3] http://casjobs.sdss.org/

[4] http://www.mpa-garching.mpg.de/SDSS/. Note that although the MPA-JHU catalog is limited to DR4 only, no loss of possible targets derived from this cut.

**Table 1.** Sample properties.

| ID | RA (J2000.0) | Dec (J2000.0) | z | $r_{petro}$ mag | L-w Age Gyr | L-w $Z$ $Z_\odot$ | M* $10^{10}\times M_\odot$ |
|---|---|---|---|---|---|---|---|
| (1) | (2) | (3) | (4) | (5) | (6) | (7) | (8) |
| PSB J0151−0056 | 01:51:07.02 | −00:56:36.78 | 0.198 | 17.50 | $1.06^{+0.02}_{-0.02}$ | $2.31^{+0.01}_{-0.35}$ | $5.26^{+0.15}_{-0.47}$ |
| PSB J0227−0015 | 02:27:43.21 | −00:15:23.08 | 0.219 | 16.92 | $1.04^{+0.69}_{-0.08}$ | $0.77^{+0.01}_{-0.07}$ | $7.06^{+2.56}_{-0.41}$ |
| PSB J0328+0045 | 03:28:02.62 | +00:45:02.43 | 0.202 | 17.50 | $1.42^{+0.02}_{-0.12}$ | $1.68^{+0.01}_{-0.01}$ | $6.86^{+0.17}_{-0.16}$ |
| PSB J0957+0249 | 09:57:29.91 | +02:49:42.02 | 0.216 | 17.37 | $0.89^{+0.01}_{-0.01}$ | $1.61^{+0.01}_{-0.01}$ | $4.96^{+0.12}_{-0.11}$ |
| PSB J1006+1308 | 10:06:21.59 | +13:08:45.91 | 0.186 | 17.30 | $1.45^{+0.29}_{-0.14}$ | $0.37^{+0.27}_{-0.05}$ | $4.30^{+0.74}_{-0.60}$ |
| PSB J1015+0103 | 10:15:19.69 | +01:03:41.68 | 0.216 | 17.22 | $0.89^{+0.03}_{-0.01}$ | $1.61^{+0.01}_{-0.37}$ | $5.31^{+0.14}_{-0.13}$ |
| PSB J1039+0604 | 10:39:34.51 | +06:04:25.00 | 0.163 | 17.13 | $0.77^{+0.01}_{-0.01}$ | $2.21^{+0.01}_{-0.01}$ | $3.14^{+0.07}_{-0.07}$ |
| PSB J1046+0714 | 10:46:19.33 | +07:14:52.34 | 0.173 | 17.59 | $1.44^{+0.42}_{-0.17}$ | $0.68^{+0.44}_{-0.26}$ | $3.42^{+0.56}_{-0.23}$ |
| PSB J1119+1313 | 11:19:49.98 | +13:13:02.54 | 0.186 | 17.09 | $0.85^{+0.01}_{-0.01}$ | $2.15^{+0.01}_{-0.01}$ | $4.66^{+0.12}_{-0.12}$ |
| PSB J1125+0049 | 11:25:55.17 | +00:49:58.82 | 0.181 | 17.43 | $1.03^{+0.01}_{-0.02}$ | $1.81^{+0.01}_{-0.01}$ | $5.66^{+0.15}_{-0.14}$ |
| PSB J1133+0205 | 11:33:49.62 | +02:05:14.90 | 0.178 | 17.41 | $1.29^{+0.54}_{-0.60}$ | $0.62^{+1.35}_{-0.29}$ | $4.41^{+0.77}_{-0.97}$ |
| PSB J1141+1014 | 11:41:15.54 | +10:14:25.68 | 0.215 | 17.63 | $1.11^{+0.64}_{-0.26}$ | $1.36^{+0.79}_{-0.72}$ | $4.43^{+1.44}_{-0.46}$ |
| PSB J1150−0107 | 11:50:01.44 | −01:07:37.02 | 0.169 | 17.79 | $0.84^{+0.70}_{-0.31}$ | $0.21^{+0.26}_{-0.13}$ | $4.51^{+1.91}_{-0.52}$ |
| PSB J1206+0918 | 12:06:30.81 | +09:18:55.09 | 0.179 | 17.58 | $1.27^{+0.35}_{-0.37}$ | $0.55^{+0.72}_{-0.25}$ | $2.67^{+0.71}_{-0.45}$ |
| PSB J1230+1038 | 12:30:54.47 | +10:38:31.63 | 0.222 | 17.69 | $0.97^{+2.34}_{-0.03}$ | $1.96^{+0.53}_{-0.02}$ | $5.10^{+5.62}_{-0.24}$ |
| PSB J1314+0430 | 13:14:14.26 | +04:30:47.65 | 0.159 | 17.14 | $1.27^{+0.03}_{-0.09}$ | $1.01^{+0.01}_{-0.03}$ | $3.79^{+0.19}_{-0.20}$ |

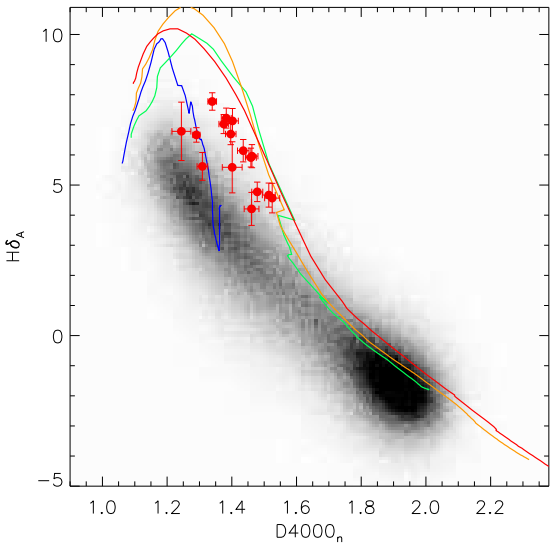


**Figure 2.** Sample properties in the classical H$\delta$-D4000$_n$ diagram, a proxy for burstiness vs. age of the stellar population. Red points with error bars are the sixteen galaxies selected for the present study; the underlying grey-scale image represents the density distribution of a complete sample of galaxies from SDSS-DR4. As one can see, our sample selects galaxies dominated by a burst in a range of young to intermediate ages. Note that the estimates of H$\delta_A$ used in this plot are not exactly the same as the E.W. measurements used in the sample selection (therefore values $< 5$ Å are not inconsistent with the selection criteria reported in the text).

ies (PSB J1039+0604, PSB J1046+0714, PSB J1119+1313 and PSB J1206+0918) have close and possibly interacting companions; in many cases, faint structures (like shells or streamers) can be tentatively seen. This suggests a relatively recent merger or interaction as a possible origin of the ceased starburst in these galaxies.

### 2.2 Observations and data reduction

The sixteen galaxies of the sample were observed in the programme ID 086.B-0733 (P.I.: S. Zibetti) at the UT3 Melipal of the ESO-VLT at the Paranal Observatory. The ISAAC instrument (Moorwood et al. 1998) has been used in two different spectroscopic setups to obtain low resolution spectra in the H and K bands. 1.5 arcsec slit and SWS1-LR grism were used in both setups, with central wavelengths of 1.65 and 2.2 $\mu$m respectively. This gives a spectral resolution of $\approx 350$ (50 Å) and $\approx 300$ (70 Å) in H and K respectively. Observations were carried out in service mode with clear (not necessarily photometric) sky and maximum seeing of 1.4 arcsec to minimise slit losses and match the fibre size and seeing of the SDSS optical spectra as well as possible. Standard ABBA on-slit nodding with 70 arcsec offsets and 20 arcsec jittering were adopted to allow accurate sky subtraction and bad pixels and cosmic ray rejection. Eight exposures of 180 sec each were taken in H band and six exposures of 150 sec each were taken in K, for total 24 minutes of integration in H and 15 minutes in K per target. This eventually yields typical signal-to-noise ratio (SNR) of $\approx 50$ and 25 per resolution element in H and K respectively. Spectro-photometric standard stars were observed with identical setup immediately after or before the science observations to provide a reliable estimate of the spectral sensitivity function and compute the corrections for telluric absorption. Standard data reduction

procedures have been implemented in IRAF[5]. Wavelength calibration has been performed based on the sky OH lines as measured on a median combined image of the scientific frames. This approach turned out to be much more stable and reliable than using the arc lamp calibrations taken in day time. We have tried different approaches to optimally correct the spectra for telluric absorption. As our best solution we adopted the following strategy: the empirical high-resolution transmissivity function of the average atmosphere above Paranal (provided by ESO) is finely tweaked by scaling and changing the resolution until we can exactly compensate for the observed absorption at various wavelengths on the spectrum of the spectrophotometric standard; the coadded spectrum of each galaxy is then corrected for the same absorption pattern as for the closest (in time and airmass) standard star. We have applied the telluric correction to both standard stars and galaxies *before* computing the sensitivity function and applying the flux calibration.

In order to assemble a SED including the visible range and the H and K NIR bands, absolute flux calibration is required. To this goal we have obtained high SNR images in $H$ and $K_s$ bands in photometric conditions with ISAAC as part of the same program. "Total" integrated magnitude derived from these images are used to rescale the spectra. By "total" magnitude we adopt the magnitude integrated within the petrosian aperture, as defined by the SDSS photometric pipeline on the SDSS $r$-band images in data release 8 (DR8, Aihara et al. 2011)[6]. DR8 is chosen as it fixes a number of issues especially with sky subtraction. $H$ and $K_s$ magnitudes are used to rescale the respective ISAAC spectra in the NIR, while the optical spectrum from the SDSS is normalised according to the $r$-band petrosian magnitude[7]. Conversions between NIR magnitudes natively calibrated in the Vega system for the ISAAC filters into the corresponding flux densities[8] for our spectra are computed based on the spectrum of Vega of Kurucz (1992), distributed by BC03. Typical total photometric uncertainties for ISAAC petrosian magnitudes are estimated $\approx 0.05$ mag and include photometric zero point fluctuations ($\approx 0.03$ mag, derived from repeated observations of standard stars during the nights) and background subtraction uncertainties.[9] For the SDSS we assume errors of 0.02 mag, which is the maximum reported for our objects by SDSS-DR8. Foreground Galactic extinction correction is finally applied using the optical depth derived from Schlegel et al. (1998) and assuming the standard extinction laws of Cardelli et al. (1989) and O'Donnell (1994).

### 2.3 Aperture effects

The spectra of our galaxies, both SDSS and ISAAC, are taken in relatively small apertures or slits centred on the brightness peak: 3-arcsec fibres are used in the SDSS with a typical seeing of $\approx 2$ arcsec while 1.5-arcsec long-slits with seeing of 1.4 arcsec or better are used with ISAAC. Relative aperture size and seeing are designed to conspire and collect a similar fraction of the galaxy light. By rescaling the spectra according to the "total" petrosian magnitudes we implicitly assume that stellar population gradients are of limited relevance and the central region of the galaxies are representative of the whole. Pracy et al. (2012) have analysed a small sample of post-starburst galaxies with integral field spectroscopy and showed that, in reality, a large fraction of them have cores that are younger than the rest of the galaxy, hence our assumption does not strictly hold. Unfortunately, because of different seeing conditions and geometry of the apertures, a precise and homogeneous rescaling of the spectra is very hard to achieve. However, by comparing fluxes and colours that are obtained in the petrosian and in the fibre apertures we can show that the aperture effects for our sample are small enough not to affect our conclusions.

First of all, we note that at the relatively high redshift of our sample the apparent size of the galaxies is typically 2.5 arcsec (median petrosian radius, maximum 3.1 arcsec), so that the 3-arcsec SDSS fibre typically collects already half of the total flux. The ISAAC spectra roughly collect the same fraction of flux. The long slit geometry in this case integrates into the spectra not only the central part, but also the outskirts of the galaxy, so that the ISAAC spectra are indeed even more representative of the whole galaxy.

In second place, we have checked by how much "total" petrosian colours differ from fibre colours in the optical. Fibre colours are computed in such a way that they correspond as closely as possible to the SED portion effectively captured in the SDSS spectra. The strongest effects are expected and observed in $g-i$, since this colour roughly corresponds to $u-r$ at $z \approx 0.2$ and therefore is the most sensitive to stellar population properties by bracketing the D4000 break. We find that, on average, fibre $g-i$ is bluer by 0.027 mag with respect to the corresponding total petrosian colours, with a rms of 0.037. Only four galaxies (out of 16) have a fibre colour which is bluer than total by more than 0.05 mag: PSB J1046+0714, PSB J1015+0103, PSB J0227−0015 and PSB J0328+0045. We dub these galaxies "blue core" in the following. For the remainder, differences in colour can be considered as not significant, although the data hint at starbursts preferentially occurring in the central regions of galaxies rather than in the outskirts, consistently with Pracy et al. (2012). Looking at $r-i$, which roughly corresponds to the rest-frame optical colour $m_{0.55} - m_{0.70}$ that subsample of our galaxies are found in good agreement within the quoted uncertainties.

[5] IRAF is distributed by the National Optical Astronomy Observatory, which is operated by the Association of Universities for Research in Astronomy (AURA) under cooperative agreement with the National Science Foundation.

[6] Data are obtained from the DR8 casjobs catalog server http://skyservice.pha.jhu.edu/casjobs.

[7] We adopt the petrosian magnitudes distributed in the SDSS-DR8. We have independently checked these values by doing our own aperture photometry on the SDSS images and found substantial agreement: our estimates are 0.011 mag fainter on average, with a scatter of 0.015 mag. Only for two galaxies (PSB J1133+0205 and PSB J0151−0056) we find fainter magnitude by more than 0.03 mag (+0.040 and +0.033 respectively). These small discrepancies are well within the errors adopted in Sec. 3.2 and 3.3.

[8] Average flux densities within broad band filters are computed according to the integral defining AB magnitudes given by Fukugita et al. (1996).

[9] Photometric measurements similarly performed on the UKIDSS (Lawrence et al. 2007) images that are available for a

will be discussed in the following, we find even smaller differences of 0.012 mag on average (0.021 mag rms). These are well within the spectrophotometric calibration errors.

Finally, we estimate the relative aperture corrections between the optical and NIR bands. Specifically, we consider the aperture corrections in $r$ and $H$-band, defined by $ap\_corr = m_{\rm fiber} - m_{\rm petro}$. For the $r$-band we use the quantities provided by the SDSS database. For the $H$-band we use the total petrosian magnitude as derived above, while to obtain fibre magnitudes we first convolve the ISAAC images to a common PSF of FWHM=2 arcsec and then integrate the flux within a circular aperture of 3 arcsecond in diameter, as done in the SDSS pipeline. Since for most of the ISAAC images we lack a sufficient number of high SNR stars to compute an accurate PSF, the final FWHM is approximated within 0.1 arcsec. We find an average difference of aperture corrections in $r$ and $H$-band $< ap\_corr_r - ap\_corr_H >= 0.026$ mag with rms of 0.1 mag, indicating that on average our galaxies are slightly more concentrated in $r$ than in $H$, although with very marginal significance. This is consistent with the existence of few blue cores and, in general, of very small systematic SED variations between the spectral and the total apertures.

This analysis of the aperture effects justifies our choice to use the total petrosian magnitude to compute the relative normalisation of the optical and NIR spectra. Total petrosian magnitudes are much more stable than magnitudes integrated in small apertures comparable with the seeing, which therefore rely on uncertain PSF convolution. On the other hand, we have shown that they do not introduce significant biases between different spectral regions. The systematic aperture bias of 0.026 mag between $r$ and $H$ is in fact well within the photometric uncertainties estimated in the previous section.

In the following analysis we will adopt 0.1 mag as standard error on the optical-NIR colours and 0.05 mag on the optical colours, to take into account both photometric errors and aperture effects.

## 3 RESULTS AND ANALYSIS

### 3.1 Composite optical-NIR spectra: absence of sharp NIR features

The composite optical-NIR spectra obtained as explained in the previous section are presented in Fig. 3, in the rest frame and normalised to the flux density at 5500 Å, in order to ease a prompt comparison between all galaxies. The actual normalisation refers to the median flux in the range 5480–5520 Å, in order to minimise the effect of noise on the individual spectral pixels. The SDSS portion of the spectra covers approximately the rest-frame range 3000–7500 Å, ISAAC H 1.25–1.50 $\mu$m, and ISAAC K 1.65–2.00 $\mu$m. For each galaxy, three panels display the full optical-NIR spectral range (top left plot), a zoom into the optical region that includes the most significant diagnostic lines (top right plot), and the NIR H–K range (bottom plot). Green lines are used to plot the spectra at high resolution: the original $\approx$ 40 and 50 Å resolution at $\approx$ 4 and 6 Å per pixel in the rest frame is used for the H and K spectra respectively, while for the SDSS spectra (original resolution 2.5 Å at $\approx$ 1 Å per pixel in the rest frame) a smoothing over 3 pixels is applied to make the plot more readable. Black thick lines are used to (over)plot heavily smoothed versions of the spectra, in order to ease the identification of possible spectral features, especially in the NIR bands: smoothing over 15 pixels is adopted both in the optical and the NIR spectra, resulting in rest frame resolution of $\approx$ 15, 60 and 90 Å in optical, H and K ranges, respectively. Vertical dotted lines mark the position of the main (expected) spectral features: the Balmer series (up to H$\eta$ 9-2) and the two features of CN (1.41 $\mu$m) and $C_2$ (1.77 $\mu$m) due to carbon rich AGB stars (Lançon & Mouhcine 2002). For each galaxy in the bottom panel we report also the light-weighted stellar age and metallicity and corresponding uncertainties derived from optical absorption features as in Gallazzi et al. (2005).

All galaxies display typical E+A or post-starburst spectra with very strong Balmer absorptions, well developed D4000 break and blue continuum. The actual slope of the optical continuum generally shows the well known dependence on age and metallicity, although dust attenuation may affect the slope as well. We do not attempt to put any constraint on this parameter, but discuss its possible impact on our conclusions below. Three galaxies, PSB J0227−0015, PSB J0328−0045, and PSB J1150−0107 show significant H$\alpha$ emission (and some higher ionisation lines for PSB J0328−0045), indicating some residual ongoing star formation, which is also confirmed by (marginal) detections at 22 $\mu$m (W4) in the WISE All Sky Survey (Wright et al. 2010), measured with SNR of 4.4 and 2.8, and 2.0, respectively. However, the equivalent width in all cases matches the Goto (2005) criteria, being $-2.27\pm0.10$ Å, $-2.80 \pm 0.10$ Å, and $-2.43 \pm 0.24$ Å, respectively, all larger than $-3$ Å. Given the observed strength of all Balmer absorption lines, the contribution of newly formed stars (or AGN) can be largely neglected in comparison to the radiation by the intermediate-age population we aim at studying here. It is worth noting that two of these galaxies (PSB J0227−0015 and PSB J0328−0045) also have a blue core, supporting the idea that blue cores might be related to some residual star formation extending close to the present time. The absence of emission lines and blue cores from the majority of the galaxies in our sample further confirms their nature of genuine post-starburst galaxies.

What is most important for the scope of this work is the lack of any evidence for sharp features in the NIR in any of the 16 galaxies. Most of them display completely featureless continua with approximately uniform slope within the two NIR windows. Some tentative evidence for a wavelength-dependent slope is seen in a few objects: PSB J1039+0604, PSB J1046+0714 and especially PSB J1314+0430 appear to change their slope around 1.41 $\mu$m, while in PSB J1119+1313 and PSB J1133+0205 a change of slope can be tentatively seen around 1.77 $\mu$m. Similar mild changes of slope, most likely due to molecular bands in the atmospheres of cool stars, are compatible with BC03 but are in fact substantially dissimilar from the sharp drops by a few 10% in flux predicted by Ma05 models (see Fig. 1).

To further support these conclusions, we stacked all 16 spectra in H and K separately, after normalising them in a 1000 Å-wide region around 1.41 and 1.77 $\mu$m, respectively. The results are displayed in Fig. 4, with the black lines show-

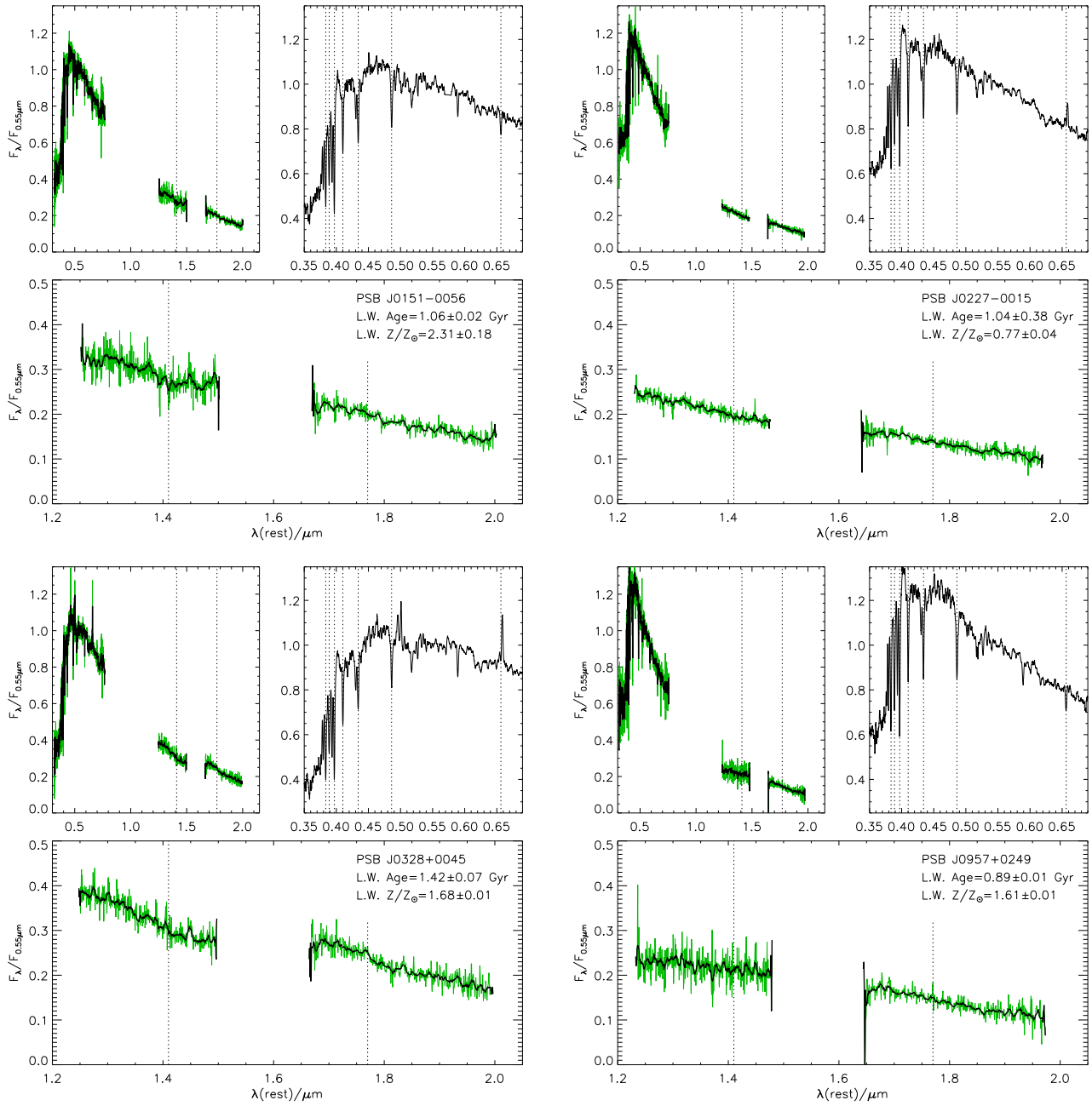


**Figure 3.** Composite rest-frame spectra for the sixteen galaxies of the sample, including optical SDSS spectra and the new NIR H and K band spectra observed with ISAAC at the ESO-VLT. Correction for foreground Galactic extinction and normalisation at 5500 Å are applied after relative normalisation between the optical and the NIR spectra based on SDSS $r$-band photometry and our own ISAAC imaging, as detailed in the text. The full/high resolution version of the spectra is plotted in green (rest-frame resolution 2.5 Å for the SDSS and 40 and 50 Å for ISAAC); the thick black curves are smoothed versions of the same spectra, to filter out the noise and improve the visibility of the features. The resulting effective resolution in these smoothed spectra is $\approx$ 15, 60 and 90 Å rest-frame in optical, H and K ranges, respectively. The new NIR H and K band spectra observed with ISAAC at the ESO-VLT are displayed in the bottom plot of each panel. The full optical-NIR range is shown in the top-left plot, while a zoom-in of the optical range is shown in the top-right plot. Vertical dotted lines mark the position of the main (expected) spectral features: the Balmer series (up to H$\eta$ 9-2) and the two features of CN (1.41 $\mu$m) and $C_2$ (1.77 $\mu$m) due to carbon rich AGB stars (Lançon & Mouhcine 2002). Light-weighted ages and metallicity are reported for each galaxy (see text for details).

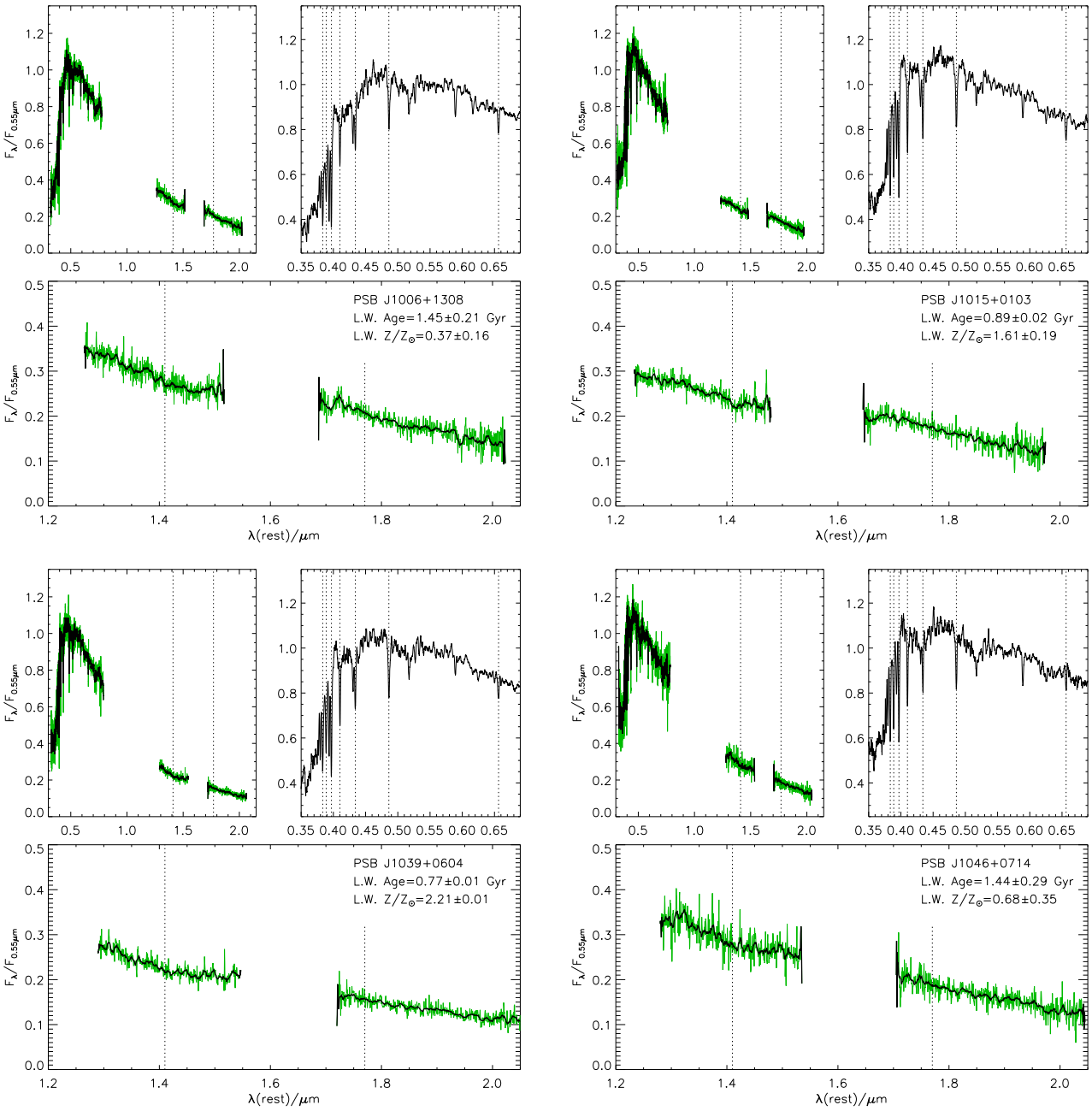


**Figure 3. (continued)**

ing the average spectrum and the shaded green area indicating the 16-84% inter-percentile range (approximately $\pm 1\sigma$ range). This figure shows that *on average* carbon molecules in the atmospheres of evolved stars produce band-head drops that are definitely less than 5% of the continuum.

### 3.2 Optical-NIR colours vs optical absorption indices

Stellar absorption indices in the optical range are extremely powerful diagnostics of stellar population properties. Decades of development and tests have led to substantial agreement on their interpretation in terms of ages and global metallicity. In this section we exploit part of the wealth of information that we can extract from the optical SDSS spectra of our galaxies for two main purposes: *i)* probe the ability of "TP-AGB light" models (represented by BC03) and "TP-AGB heavy" models (Ma05) to reproduce the observed trends and distributions in the parameter space of optical absorption indices and optical-NIR colours; *ii)* investigate whether the lack of NIR spectral features can be due to selection biases such that we misinterpreted optical diagnostics (e.g. due to the use of BC03-based model libraries) and ended up missing the relevant phase for TP-AGB stars.

We start considering only age-sensitive absorption in-

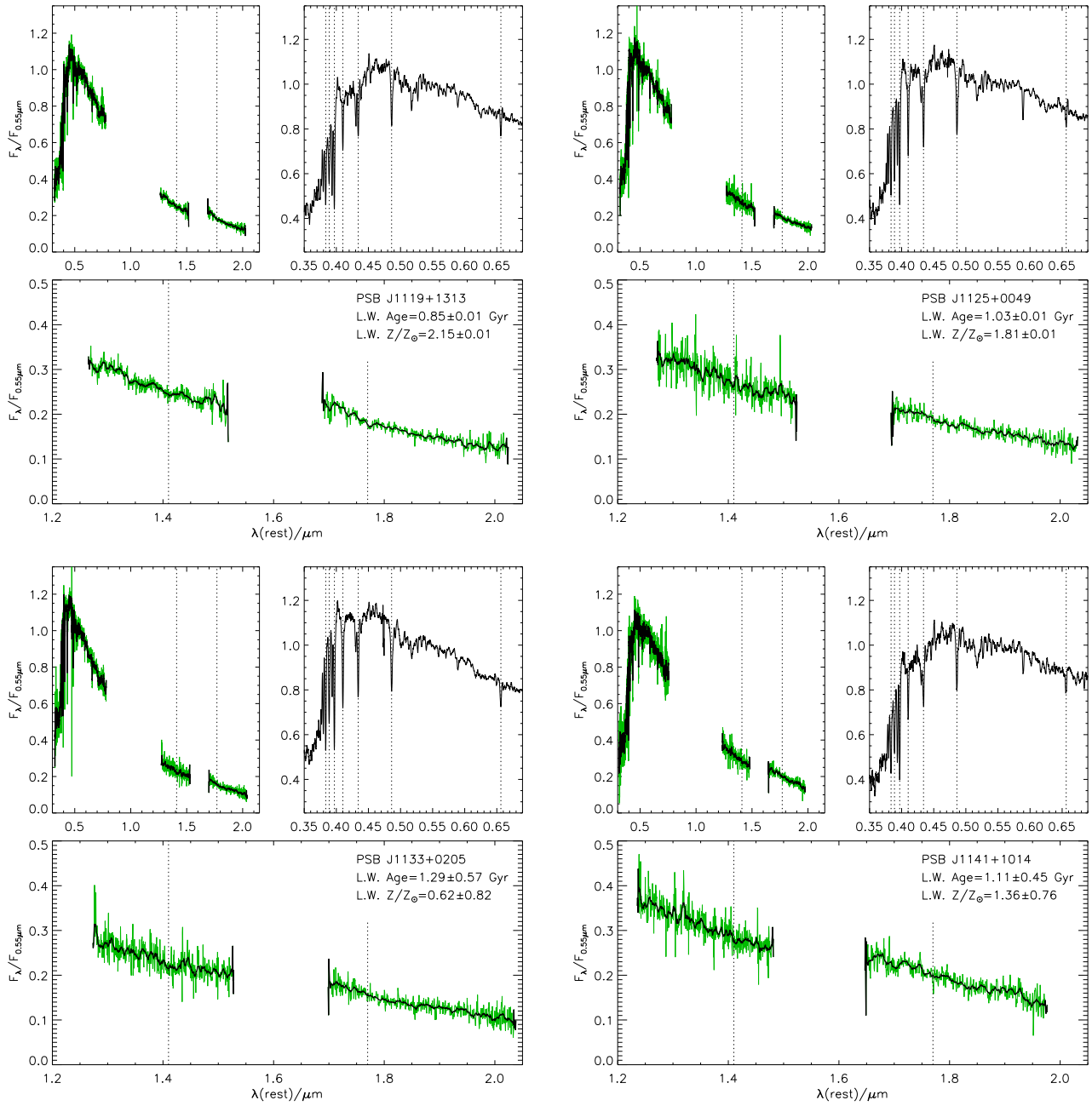


**Figure 3. (continued)**

dices and optical-NIR colours and build the diagnostic plots presented in Fig. 5 for BC03 and Ma05 in the *top row* and *bottom row*, respectively: coloured symbols and lines show the predicted optical-NIR colour $m_{0.55} - m_{1.40}$ as a function of $H\delta_A + H\gamma_A$, $D4000_n$, and the optical colour $m_{0.55} - m_{0.70}$ (from *left* to the *right*).[10] For BC03, ages range from 50 Myr (lower ages are not relevant for the present analysis as they would yield much bluer colours than observed) to 13.6 Gyr. Metallicities range from 1/50 solar to 2.5 times solar, and are represented with different symbols and colours from blue to red (solar in orange, see figure caption). Symbols of increasing size are used to mark discrete increasing ages, with the crucial age of 1 Gyr identified by a star. The spectral indices $H\delta_A + H\gamma_A$ and $D4000_n$ are measured after convolving the model spectra to match the resolution and average velocity dispersion of the galaxies ($< \sigma >= 164$km s$^{-1}$). The Ma05 SSP spectra are distributed over the full optical-NIR range only at low resolution (20 Å sampling), therefore cannot be used to compute reliable indices, $H\delta_A + H\gamma_A$ in particular.[11] Maraston & Strömbäck (2011) delivered high reso-

[10] Here $m_{0.55}$, $m_{0.70}$ and $m_{1.40}$ denote the AB magnitudes corresponding to the flux density around 0.55, 0.70 and 1.40 $\mu$m (rest), respectively.

[11] The effect of such a coarse sampling is to underestimate

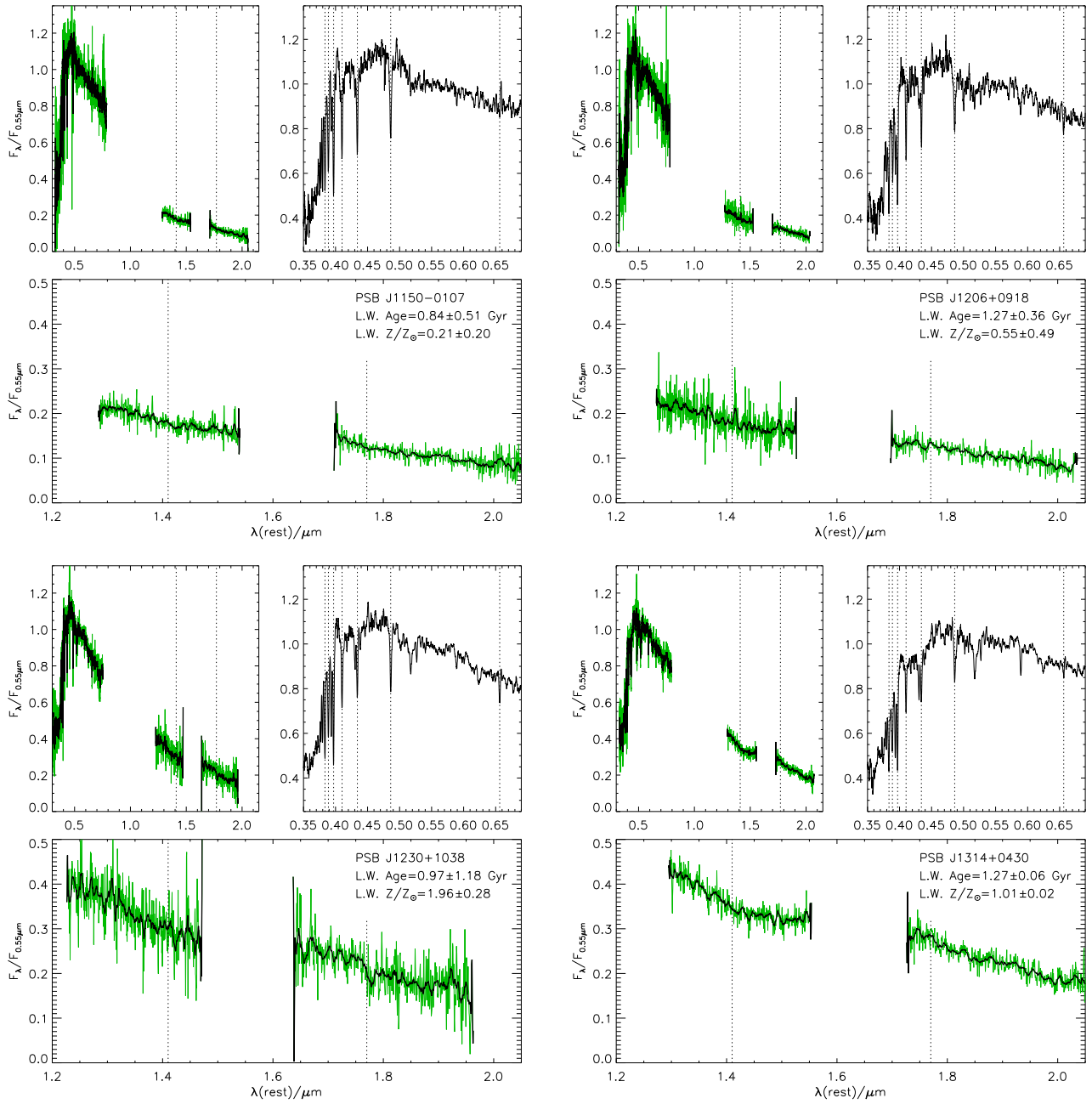


**Figure 3. (continued)**

lution spectra for a subsample of the Ma05 age-metallicity grid, over the optical range: only three metallicities are available (0.5, 1.0 and 2.0 solar), with the lowest ages being 200, 30, 400 Myr, respectively. We use these models (in their STELIB version), convolved to the effective resolution of our data, to compute the $H\delta_A + H\gamma_A$ and $D4000_n$ plotted in the first two panels of the *bottom row* of Fig. 5; optical-NIR colours are computed from the original Ma05 SEDs of corresponding age and metallicity. For the colour-colour plot the full grid of Ma05 is used instead, which allows extending the metallicity down to 1/20 solar and the age down to 50 Myr as for BC03. Observational data points derived from our composite optical-NIR spectra are plotted as error bars.[12]

$H\delta_A + H\gamma_A$ by up to $\approx 5$ Å and to overestimate $D4000_n$ by up to $\approx 0.1$.

[12] Errors on the colours are uniformly set equal to 0.05 and 0.1 mag for the optical colour $m_{0.55} - m_{0.70}$ and the optical-NIR colour $m_{0.55} - m_{1.40}$ respectively, following the discussion in Sec. 2.3. Errors on indices are derived from the MPA-JHU catalog and, in the case of $D4000_n$, incremented *a posteriori* to take into account flux calibration errors, as statistically derived by comparing duplicate observations of a large sample of SDSS galaxies.

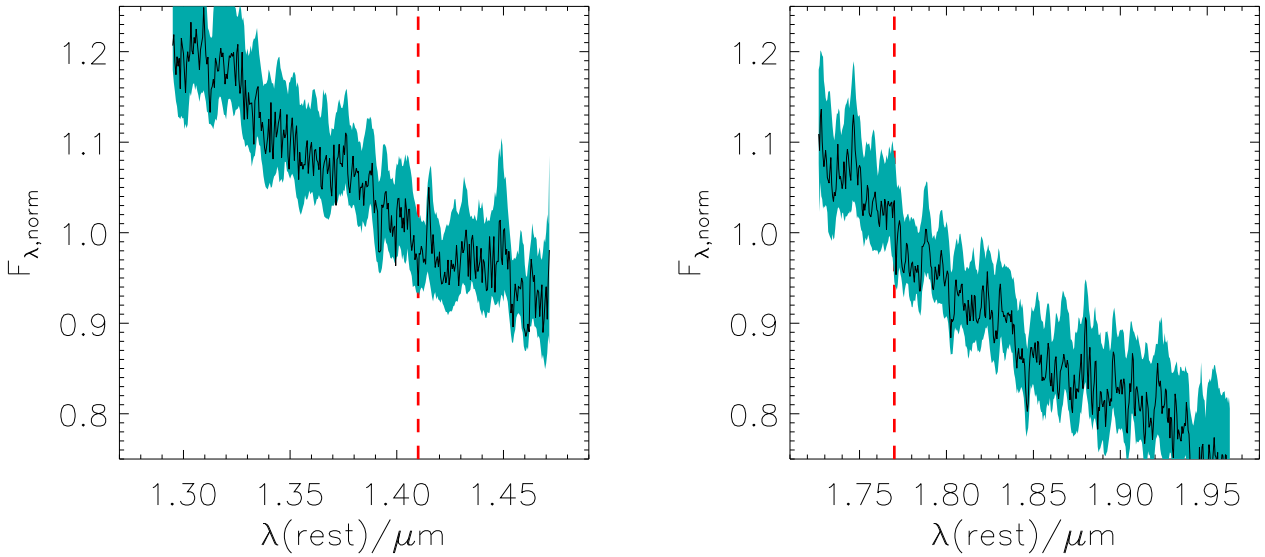


**Figure 4.** Stacked H (*left panel*) and K (*right panel*) spectra of the 16 galaxies. Each spectrum has been re-normalized to 1 in a wavelength range of 1000 Å around the expected positions of the features at 1.41 and 1.77 $\mu$m (marked with red dashed vertical lines), respectively. Band-head drops of more than a few per cents *on average* can be ruled with very high confidence.

As shown by the *top* row of Fig. 5, BC03 SSPs provide a good match to the observed spectral diagnostics, with the only exception of a couple of galaxies, PSB J1150−0107 and PSB J1206+0918, which appear to have a too blue $m_{0.55} - m_{1.40}$ NIR-optical colour for the given $m_{0.55} - m_{0.70}$ optical colour (or, reversely, a too red $m_{0.55} - m_{0.70}$ for the given $m_{0.55} - m_{1.40}$) and will be discussed in Sec. 3.4. In particular, galaxies cover the range in age and metallicity corresponding to light-weighted ages and metallicities listed in Table 1, which are mostly relevant for the TP-AGB phase.

As far as the comparison with the Ma05 models is concerned, we note that the observed age-sensitive indices approximately match the range of ages given by our light-weighted estimates. Most of the observed $H\delta_A + H\gamma_A$ and $D4000_n$ values correspond to SSP ages between 0.5 and 1 (1.5) Gyr for the solar (sub-solar) metallicity track, while ages smaller than 0.5 Gyr would be inferred from the 2 times solar metallicity track. For the given indices, however, the predicted $m_{0.55} - m_{1.40}$ NIR-optical colours are on average 0.5 mag redder than the observed ones. This is consistent with the Ma05 "TP-AGB heavy" models having the NIR very much boosted with respect to BC03 in the age range around 1 Gyr implied by the Balmer indices. In the rightmost panel of Fig. 5, *bottom* row, we see that, unless a metallicity as low as 1/20 solar is representative of most galaxies and ages are significantly larger than 1 Gyr, the Ma05 models predict $m_{0.55} - m_{1.40}$ NIR-optical colours that are on average 0.5 mag redder than observed, for the observed optical $m_{0.55} - m_{0.70}$ colours.[13]

We note that the inclusion of dust with a standard effective attenuation curve in the models does not alleviate the tension between the Ma05 models and observations. We illustrate this in Fig. 5 by drawing arrows which represent the offset to apply to each model when an optical extinction of $A_V = 1$ mag and an effective attenuation law $\tau_\lambda \propto \lambda^{-0.7}$ (following Charlot & Fall 2000, for an SSP) are applied. As expected, the effect of dust is to move model tracks to redder colours: this would worsen the disagreement in the index-colour planes. The reddening vector is approximately parallel to the model tracks in the colour-colour plane: accounting for dust attenuation in the models would not substantially change the (dis)agreement with the observations in terms of colours, although it would require even lower metallicities and ages.

The hypothesis of a metallicity as low as 1/20 solar is not only unlikely to apply to a full sample of relatively massive galaxies with $M^* \approx 5 \times 10^{10} M_\odot$, but is also inconsistent with direct metallicity constraints which can be derived from absorption indices. In Table 1 we already showed metallicity estimates derived from the vast library (based on BC03) and bayesian method of Gallazzi et al. (2005): these estimates range from 0.2 $Z_\odot$ minimum to 2.3 $Z_\odot$ maximum, roughly uniformly distributed. In Fig. 6 we show that metallicities as low as 1/20 solar are indeed ruled out already from a simple comparison of standard absorption line indices on which different models are in substantial agreement, namely $[MgFe]'$ and $H\beta$. $[MgFe]'$ in particular is chosen as optimal metallicity indicator following Thomas et al. (2003) who demonstrated its insensitivity to $\alpha$/Fe abundance ratio; $H\beta$ serves to constrain the age of the stellar population and hence alleviate the well known age-metallicity degeneracy. Fig. 6 shows the indices measured in our galaxies as crosses with error bars, while tracks of different colours are derived from BC03 SSPs in the age range 50 Myr – 13.6 Gyr (symbols are the same as in Fig. 5). Four different metallicities, 1/50, 0.4, 1 and 2.5 solar are plotted in purple, blue, green orange and red, respectively. It is apparent from this plot that metallicities significantly lower than 0.4 solar are inconsis-

[13] Similar conclusion is reported by Conroy & Gunn (2010) concerning the colours of their sample of PSB galaxies.

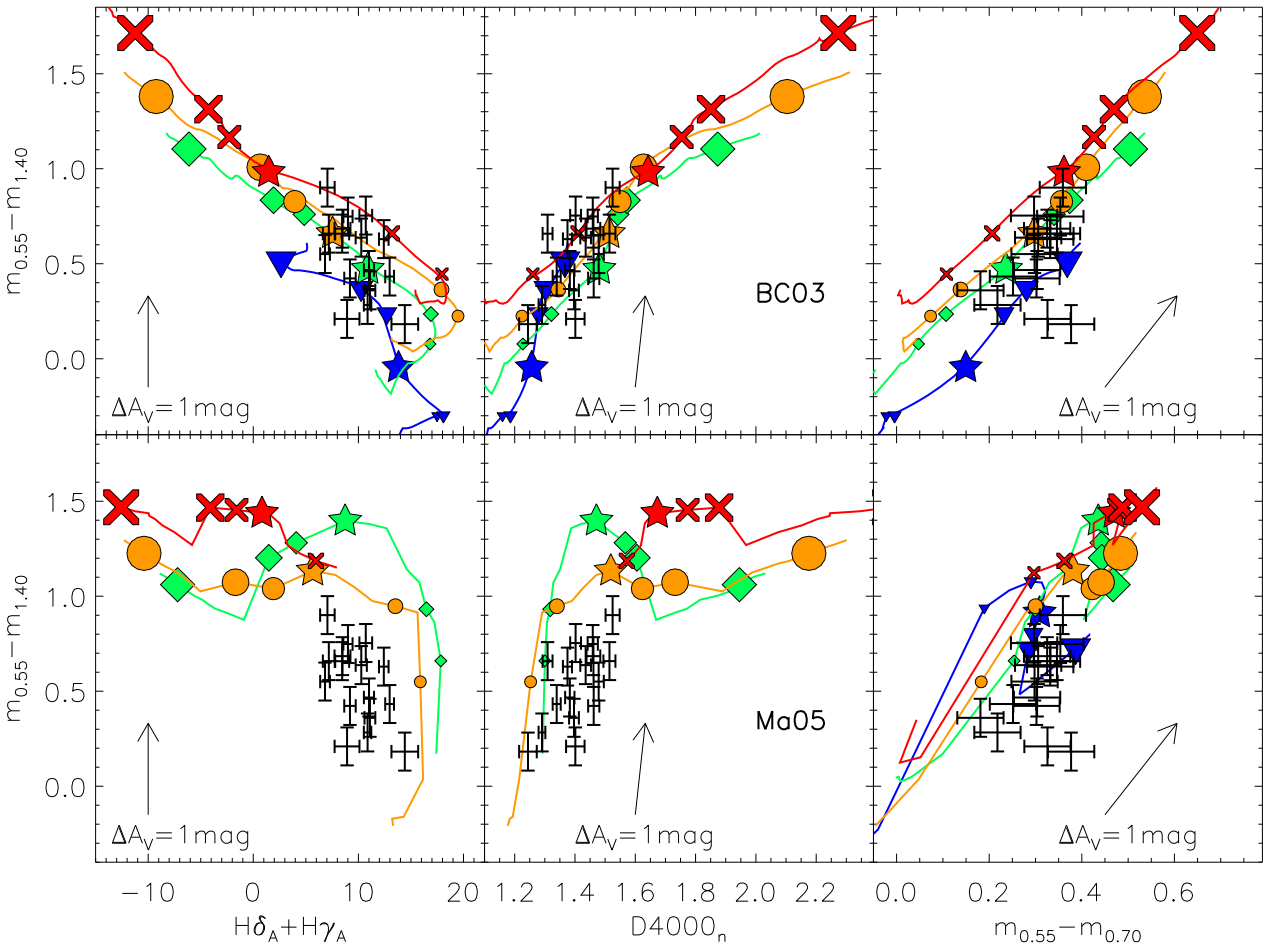


**Figure 5.** Comparison between the observed properties of the post-starburst galaxies in our sample (points with error bars) and a suite of SSP models (coloured symbols and lines) from BC03 (*top row*) and Ma05 (*bottom row*). The optical-NIR colour $m_{0.55} - m_{1.40}$ is plotted against $H\delta_A+H\gamma_A$ (*left panels*), $D4000_n$ (*central panels*), and the optical colour $m_{0.55} - m_{0.70}$ (*right panels*). Each track (blue with upside-down triangles, green with diamonds, orange with circles and red with crosses) corresponds to metallicity of 1/50, 0.4, 1 and 2.5 solar, respectively, for the BC03 models in *top row*, and to metallicity of 1/20, 0.5, 1 and 2 solar, respectively, for the Ma05 models in *bottom row*. The tracks for BC03 and the colour-colour plot of Ma05 extend from 50 Myr to 13.6 Gyr. As Ma05 only provides low-resolution SEDs, $H\delta_A+H\gamma_A$ and $D4000_n$ for these models are taken from the corresponding STELIB-based SSPs published by Maraston & Strömbäck (2011), limited to three metallicities, 0.5, 1.0 and 2.0 solar, and starting with ages of 200, 30, 400 Myr, respectively. Stars mark 1 Gyr, while symbols of increasing size mark ages of 0.3, 0.5, 1.5, 2 and 10 Gyr. IMF is assumed Salpeter in all cases. The arrow in each plot shows the shift produced by $A_V = 1$ mag for a uniform attenuation following $\tau_\lambda \propto \lambda^{-0.7}$. While colours and spectral indices can be reproduced simultaneously by BC03 SSPs, Ma05 SSPs yield optical-NIR colours that are inconsistent with age-sensitive spectral indices and optical colours, unless metallicities as low as 1/20 solar are advocated for all galaxies.

tent with the data-points. We have checked that the same conclusions are obtained if indices based on BC03 models are replaced with those computed by Thomas and collaborators (Thomas et al. 2003, 2004; Korn et al. 2005): the only difference between the two sets of models is that Thomas' models shift the lower limit allowed by the data to slightly higher metallicities.

### 3.3 Effects of composite stellar populations

A possible explanation why the strong TP-AGB features predicted by Ma05 models are not seen in our spectra is that in the NIR there is a substantial contribution by old stars, which are almost completely outshined by the younger population in the optical bands. In fact, it is quite unlikely that the entire stellar population of galaxies as massive as several $10^{10} M_\odot$ is formed in a burst $\approx$ 1 Gyr old and a more realistic scenario is that the burst shines atop an old component. To explore this hypothesis we have repeated the test presented in Fig. 5 using composite stellar populations (CSP) instead of SSPs.

In a first experiment, each CSP is composed of two components: a fixed 10-Gyr old, solar metallicity SSP (which we will call "old component" in the following) and an SSP of variable age, from 50 Myr to 13.6 Gyr, and metallicity, from 1/20 to 2–2.5 solar (which we will call "young" component or "burst", and corresponds to the SSPs of Figure 5). In the following we refer to these models as CSP-S,

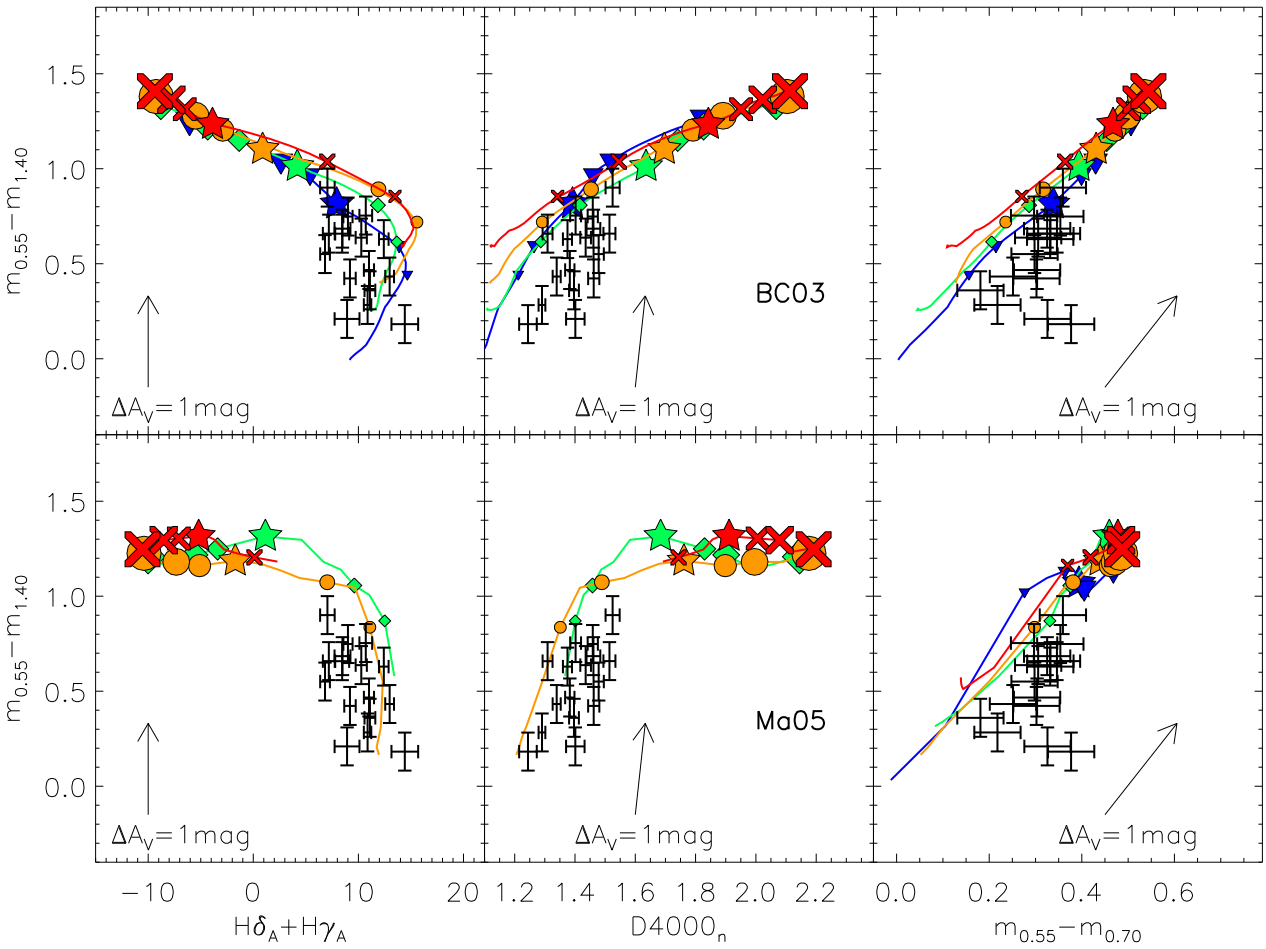


**Figure 7.** Same as Figure 5, but now using the composite SPs that are referred to as CSP-S in the text: a 10 Gyr old, solar metallicity component is combined with SSPs with the same properties as (and represented as) in Figure 5. The ratio of masses *as formed* in the fixed "old" vs variable "young" components is 9:1. For both BC03 and Ma05 models, such a combination can reproduce the spectral indices with "young" components younger than $\approx 0.5-1$ Gyr (even more so for the Ma05 models); however the optical-NIR colours cannot be reproduced by these models. Inclusion of standard dust attenuation (illustrated by the arrows) does not help also in this case.

where "S" indicates that the metallicity of the old component is solar. This choice appears reasonable considering that $Z \gtrsim Z_{\odot}$ is typical for the old component of massive galaxies with $M^* \gtrsim 10^{10} M_{\odot}$ (e.g. Gallazzi et al. 2005; Thomas et al. 2005). We have varied the relative fraction of (initial) mass in the old component and in the burst from 0:1 to 0.9:0.1. Fig. 7 shows the same diagnostic plots we already used to analyse pure SSPs (Fig. 5), but now plotting CSP-S models for the extreme "contamination", i.e. for 90% of the formed mass in the old component and 10% in the burst (as was also assumed by Conroy & Gunn 2010). Symbols and colours are the same as in Fig. 5 and refer to age and metallicity of the variable burst component alone. CSP-S models, either BC03 or Ma05, can easily reproduce the distribution of data-points in $H\delta_A + H\gamma_A$ and $D4000_n$: the contamination by the old component is compensated by a younger burst component ($\lesssim$ 500 Myr) with respect to those that provided the best match in the pure burst (SSP) models. Such a combination would easily explain why we do not see the sharp NIR features due to TP-AGB stars predicted by Ma05: not only part of the NIR emission is provided by the old and TP-AGB free stellar population, but also the young component is younger that the peak of the TP-AGB phase.

However, problems arise when optical-NIR colours are considered. The addition of an old component at solar metallicity to a young burst yields significantly redder optical-NIR colours with respect to a pure burst. As a consequence, BC03 models, which provided a decent match in the case of a pure SSP, are now shifted to inconsistently red colours with respect to the observations. In the case of Ma05 models, which already had troubles being too red in optical-NIR colours at almost any age, they become inconsistent with the observed colours of almost all galaxies. Mixtures with an intermediate mass ratio between the old population and the burst produce also intermediate results in terms of indices and colours between the pure burst models (Fig. 5) and the CSP-S ones presented in Fig. 7. In fact, as shown in Fig. 8, a more moderate ratio between "old" and "burst" stars of 2:1 yields a decent match between the BC03 models and the observations. As for the Ma05 models, however, the fact

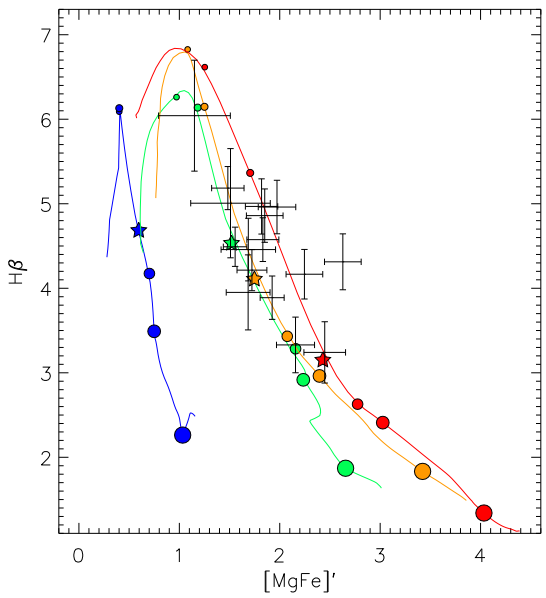


**Figure 6.** H$\beta$ vs [MgFe]$'$ diagnostic plot, showing that our galaxies need to have metallicity not lower than $\approx 40\%$ solar in order to be consistent with the observed strength of metal sensitive absorption lines. The four evolutionary tracks in colour are from BC03 models, colour coded and marked as in Fig. 5.

that already SSPs are too red in optical-NIR colours results in no combination of "old" vs "burst" stars being able to reproduce the observed colours.

We repeated the experiment with the 9:1 ratio, but changing the metallicity of the old component from $Z = Z_{\odot}$ fixed to a variable metallicity that matches the one of the "young" component. We tag these models as CSP-Y, where "Y" indicates that the metallicity of the old component is the same as in the young component. The results are shown in Fig. 9. BC03 models (Fig. 9 *top*) are able to cover most of the parameter space occupied by the data-points; however a significant number of galaxies are too blue in $m_{0.55} - m_{1.40}$ with respect to models at given $D4000_n$. Moreover, the metallicities implied by colours are systematically lower (and to large extent inconsistent) with those implied by the absorption indices alone. As one can argue in the light of the results of pure SSP and 2:1 ratio models, less extreme fractions of the old component can provide a much better match to the data. As for the Ma05 models, Fig. 9 *bottom* shows that not even with this kind of mix it is possible to match the distribution of $m_{0.55} - m_{1.40}$ vs $D4000_n$, the optical-NIR colours of the models being too red with respect to the data. We reiterate that any dust with the most commonly adopted attenuation curves would only worsen this disagreement.

In summary, adding a substantial fraction of old stellar populations to reduce the impact of TP-AGB stars predicted by Ma05 in the NIR may indeed explain the lack of observed NIR features, while remaining consistent with the observed optical spectral indices. However, such a combination fails to reproduce the observed optical-NIR colours at given $H\delta_A + H\gamma_A$, $D4000_n$ and optical colours, no matter if the metallicity of the "old" component is the same as the one of the "young" component or is fixed at the solar value (as it is probably more realistic for an old stellar population in a system of a few times $10^{10} M_{\odot}$). We cannot exclude that more complicated and *ad hoc* star formation histories and metallicity mixtures might be able to produce a closer match between observations and Ma05, but it appears unlikely that such a fine tuning actually applies to all 16 galaxies in the sample. On the other hand, BC03 models appear to reproduce the observations much more easily by assuming SSPs or CSPs with even massive "old" components of variable sub-solar metallicity; in order for models with an "old" component at solar metallicity to match the observations, "old" fractions less than 0.9 are required in most cases: it is sufficient to lower such fraction to 0.6-0.7 in order to obtain a generally good agreement.

We further illustrate these points by directly comparing SSP and CSP model spectra with an actual spectrum of our PSB sample in Fig. 10, where PSB J1006+1308 is used as a mere example which optimally serves to this goal, as it is broadly representative of the full sample. For both BC03 (shown in the left-hand panel) and Ma05 (in the right-hand panel), we pick the best fitting models from each of the three grids of SSP, CSP-S and CSP-Y (assuming old:young=9:1). They are overplotted to the observed spectrum (solid black line), in blue for the SSP, in solid red for the CSP-S and dashed green for the CSP-Y. The "best fitting" models are those yielding the minimum $\chi^2$ over the optimal set of optical absorption indices defined in Gallazzi et al. (2005) ($D4000_n$, $H\delta_A + H\gamma_A$, H$\beta$, [MgFe]$'$, [$Mg_2$Fe]). Due to the coarse grid in metallicity, the use of fixed old fractions and the neglect of dust attenuation, we warn the reader not to over-interpret these fits in terms of derived physical parameters. Nonetheless, the following key observations can be derived from Fig. 10. *i)* All best fit models can reproduce the observed optical features extremely well (see insets). The slope of the optical continuum is also generally well reproduced, although for BC03 the SSP fit is too blue in the optical range, which might be due either to a small mismatch in metallicity because of the coarse grid or to small amounts of dust, which are not included in our simple models. *ii)* The NIR spectrum of the best fitting Ma05 SSP, with an age of 0.6 Gyr and metallicity 2 times solar, has the typical NIR boosting due to the Ma05 implementation of the TP-AGB phase, clearly recognisable from the sharp features around 1.41 and 1.77 $\mu$m. However, no evidence of such features appears in the observed spectrum; moreover, the observed spectrum is almost a factor of two dimmer than the Ma05 SSP in the NIR. In contrast, the BC03 SSP provides a very good fit in the NIR both in terms of (lack of) features and of overall flux. *iii)* The use of CSPs with a substantial fraction (90%) of 10-Gyr old stars yields a relative enhancement in the NIR over optical for BC03 models, for both CSP-S and CSP-Y. The plot suggests that a smaller old fraction and lower metallicity than the best fitting pure SSP might provide a very close match to the NIR-to-optical ratio. CSPs for Ma05 (which by coincidence converge to the same solution for both CSP-S and CSP-Y, i.e. the solid red line and the dashed green one overlap) do actually yield much weaker NIR features and also lower NIR flux relative to optical. However, this stays significantly higher ($\approx 50\%$) than observed.

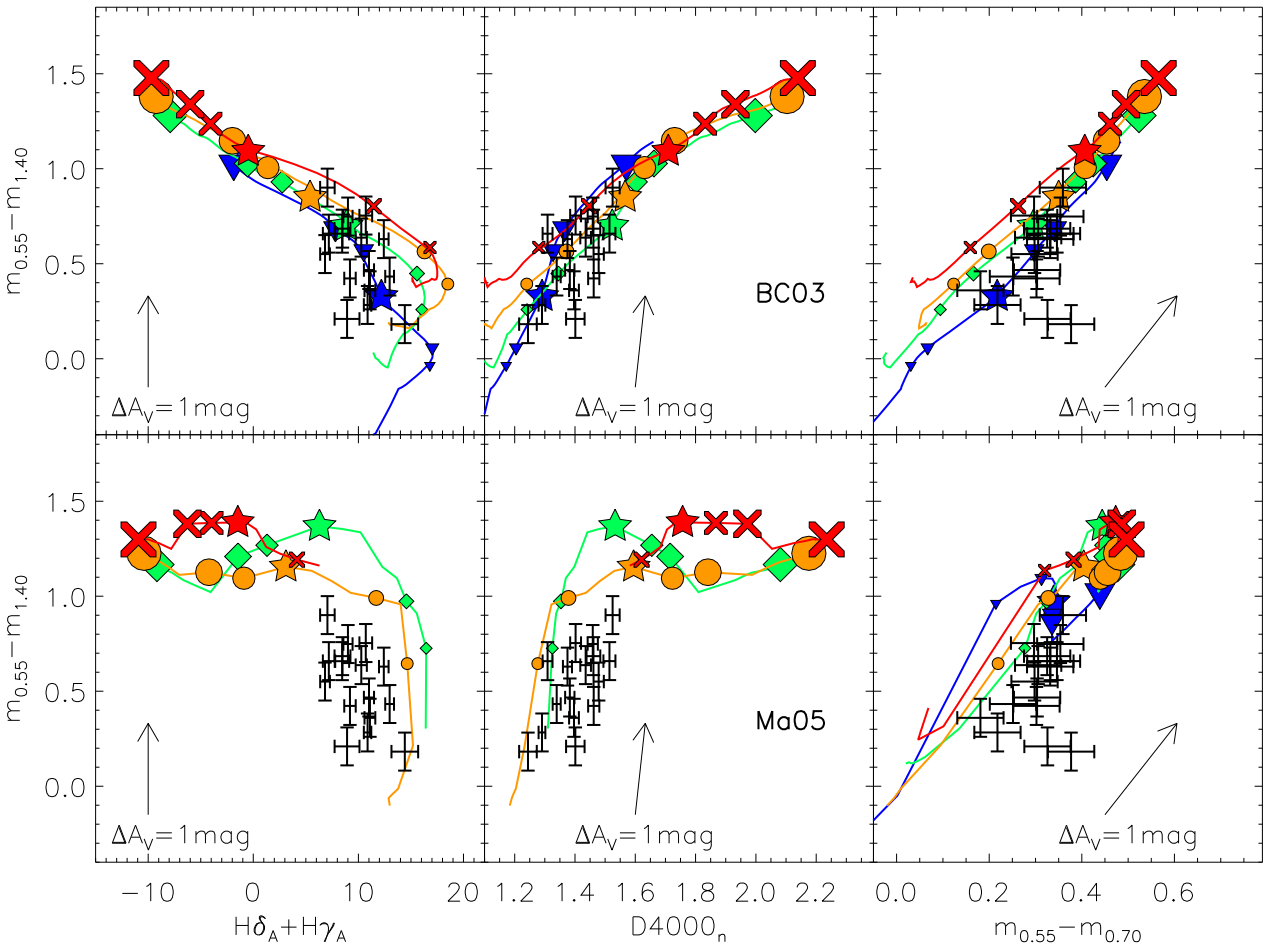


**Figure 8.** Same as Figure 7, but now using CSP-S with a ratio of masses *as formed* in the fixed "old" vs variable "young" components of 2:1. This figure shows that a substantial underlying old stellar population is compatible with most of the observations if BC03 models are used, but produces inconsistent colours if the Ma05 are adopted instead.

### 3.4 The anomalous galaxies PSB J1150−0107 and PSB J1206+0918

PSB J1150−0107 and PSB J1206+0918 are characterised by extremely blue optical-NIR colours ($m_{0.55} - m_{1.40} \lesssim 0.2$) and intermediate/red optical colours ($m_{0.55} - m_{0.70} \gtrsim 0.3$). When plotted on the colour-colour diagrams of Fig. 5, 7, 8 and 9, they significantly depart from the sequences both of observed data-points and model tracks. None of them is able to reproduce such a combination of intermediate/red optical colours and very blue optical-NIR ones: for the given $m_{0.55} - m_{1.40}$, an offset of −0.1 to −0.2 mag in $m_{0.55} - m_{0.70}$ would be required to bring them back in agreement with the models, or, for the given $m_{0.55} - m_{0.70}$, an offset of $\gtrsim 0.3$ mag in $m_{0.55} - m_{1.40}$. From the arrows plotted in the colour-colour diagrams, it is immediate to see that a standard effective attenuation à la Charlot & Fall (2000) is unable to move the models closer to these two objects: in fact, one would need an effective attenuation curve which is extremely flat, thus causing similar attenuation at 0.70 and 1.40 $\mu$m. With standard dust grains, for which the absorption cross section decreases with wavelength, this can be only obtained by invoking a peculiar geometry in which back scattering plays a major role.

Significant residual star formation is witnessed in PSB J1150−0107 by EW(H$\alpha$)= $-2.43 \pm 0.24$ and a marginal detection at 22 $\mu$m in the WISE all-sky survey. PSB J1206+0918, however, does not display any sign of star formation, with EW(H$\alpha$)= $-0.65 \pm 0.26$ and no detection at 22 $\mu$m. This suggests that residual star formation or processes related to nuclear activity are not the cause of the anomaly common to these two galaxies.

We note that the shape of the spectra of these two galaxies is peculiar in two main aspects: *i)* the continuum appears to bend down, i.e. the slope becomes steeper, going from $\approx 0.55$ to 0.8 $\mu$m, whereas all other galaxies display an approximate constant slope or even an up-bending shape in this region; *ii)* a significant and featureless drop long-ward of $\approx 0.5$ $\mu$m is observed instead of the Fe and Mg absorption complexes, which is probably due to the low metallicity of these two galaxies, among the lowest of the entire sample. These two features appear to be responsible for the anomalous colours, by making the spectral slope between 0.7 and 1.4 $\mu$m too steep relative to the one in the optical range

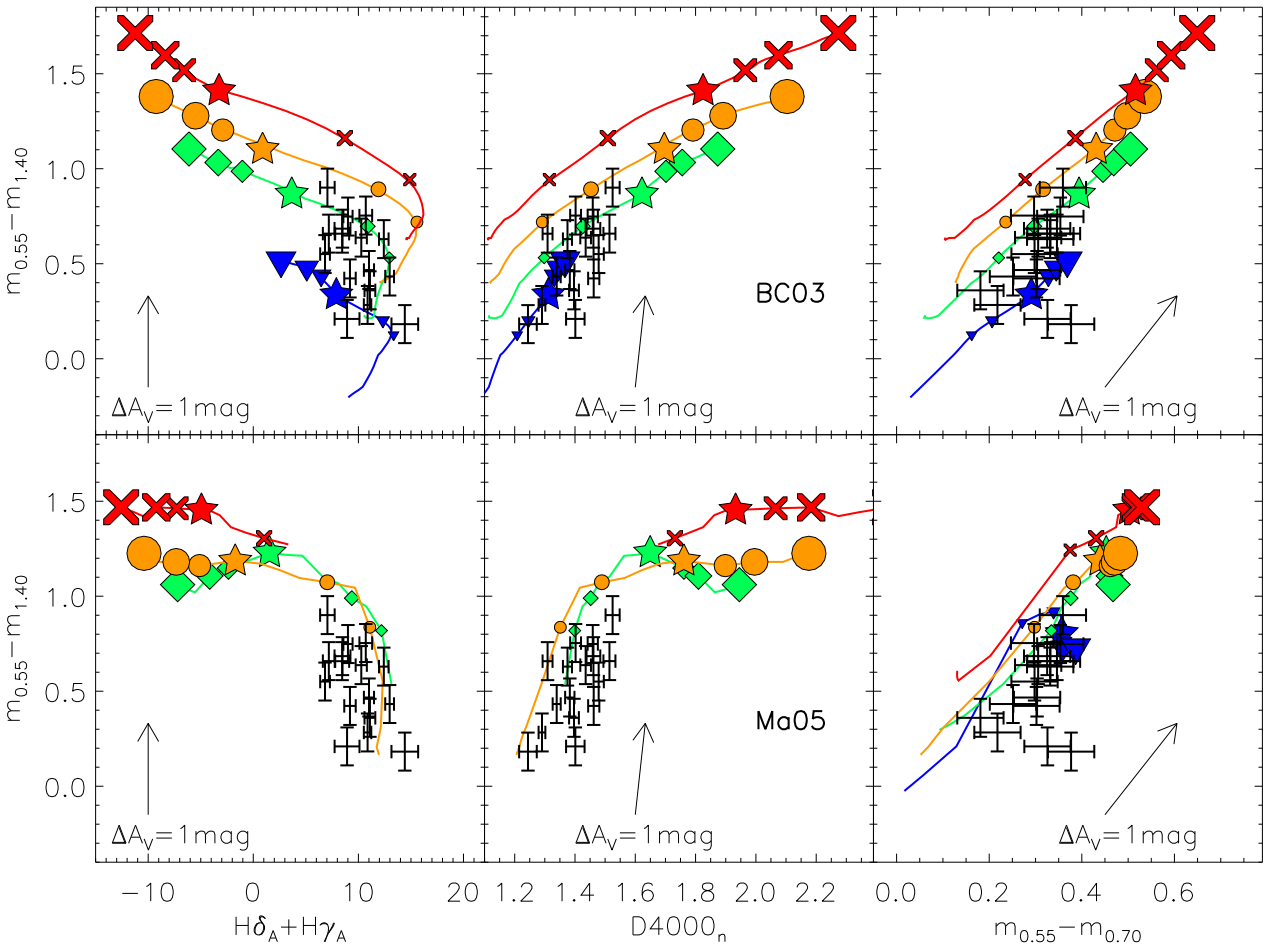


**Figure 9.** Same as Figure 7 for CSP-Y models (see text), composite SPs with the "old" component having the same metallicity as the "young" one, according to the corresponding track.

0.55–0.70 $\mu$m. The fact that models fail to reproduce these colours may point to problems in the low metallicity regime, below $\approx 0.5 Z_{\odot}$.

We note that, according to the Ma05 models, the largest enhancement and the most dramatic features in the NIR are expected for $Z \lesssim Z_{\odot}$. Instead these two low-metallicity galaxies exhibit bluer optical-NIR colours than even "TP-AGB light" models (e.g., BC03).

### 3.5 Comparison with Kriek et al.(2010)

As already mentioned in Sec. 1, Kriek et al. (2010) have obtained a detailed (rest-frame) UV-optical-NIR SED for a sample of 62 PSB galaxies observed in the *NEWFIRM* Medium Band Survey (NMBS) in the redshift range 0.7–2. Their composite SED is essentially a stack of the SED of their sample. They applied maximum likelihood fitting using both BC03 and Ma05 on different wavelength ranges (optical only or optical plus NIR) and, similarly to the results we have presented in this work, they found that Ma05 cannot reproduce the blue optical-NIR colours observed, whereas BC03 provide an almost perfect match.

In Fig. 11 we compare the SED published by Kriek et al. (2010), represented by the red points with error bars, with the stack of our 16 spectra. Both SEDs are normalised at 5500 Å. The black line is the median of our 16 spectra at each wavelength, while the shaded area displays the 16–84 inter-percentile range. The similarity of the stacked SEDs from the two works is striking, typically consistent within 1–1.5 $\sigma$. Our spectra are slightly bluer and steeper in the range 5000 Å to 2 $\mu$m, which might derive from some relative bias in the respective sample selections., with our objects being somehow more extreme (e.g. in terms of burst fraction, see also Sec. 4). In fact, Kriek et al. (2010) define their sample based on k-corrected rest-frame colour cuts which are hardly comparable to our spectroscopic criteria. Alternatively, this comparison might indicate that NIR-bright evolved (TP-AGB) stars have a slightly larger influence on the SED of PSB galaxies at $z \gtrsim 0.7$ than at $z \approx 0.2$, consistently with expectations, e.g., of Melbourne et al. (2012). Apart from this minor colour difference, our detailed spectroscopic study of individual PSB galaxies confirms and reinforces the previous results by Kriek et al. (2010), based on stacking and medium band photometry and at a very different age of the Universe.

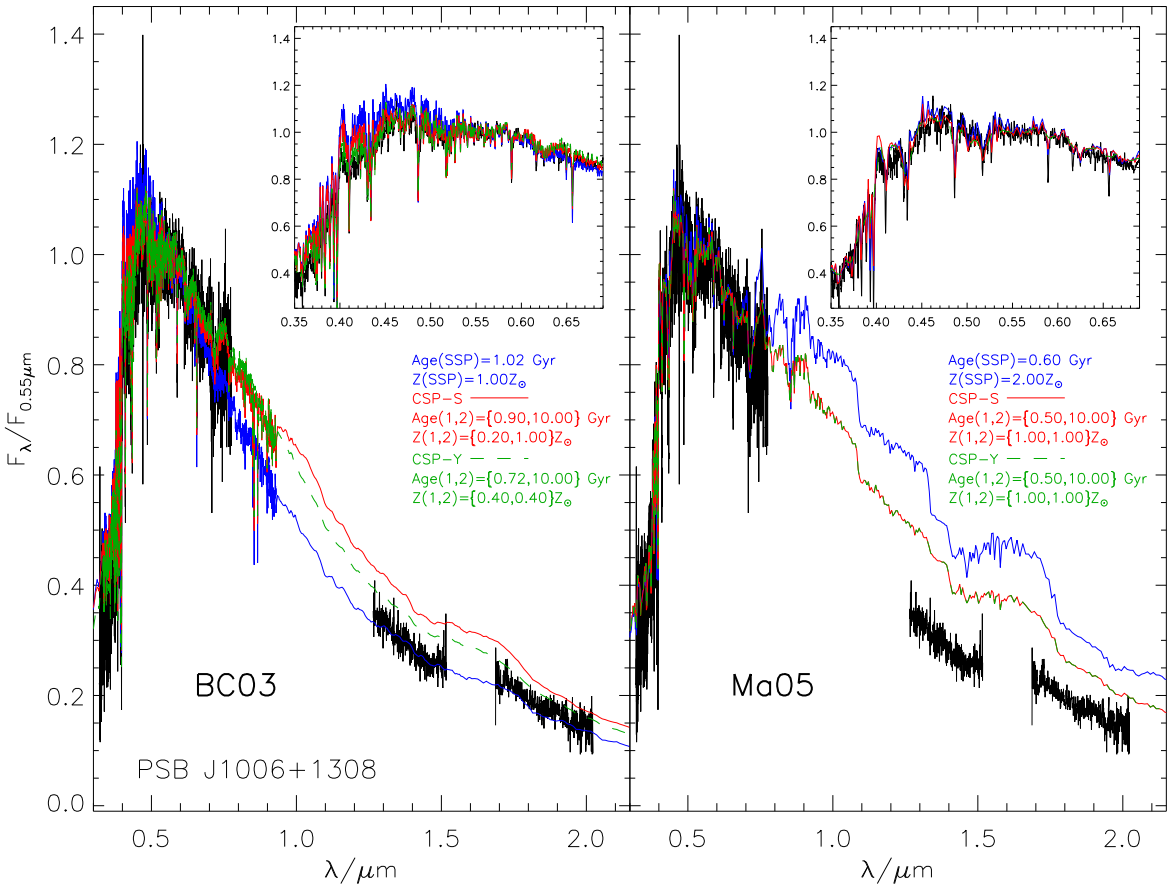


**Figure 10.** Example of how different models perform in reproducing the SED of a PSB galaxy, specifically PSB J1006+1308, whose *observed* spectrum is shown in black. In the left-hand panel models based on BC03 are overplotted, while models based on Ma05 are shown in the right-hand panel: the blue lines are used for pure SSP, red solid lines for CPS-S (90% 10-Gyr old component at solar metallicity) and green dashed lines for CSP-Y (90% 10-Gyr old component at the same metallicity as the young component). The models plotted here are chosen from each of the simple grids presented in the text and in Fig. 5, 7 and 9 as those that best fit the set of five optical stellar absorption features sensitive to age and metallicity defined in Gallazzi et al. (2005). All models can reproduce the spectral absorption features remarkably well (see insets) and agree on the presence of a young component approximately at the peak of the TP-AGB contribution. However their extrapolations to the NIR regime differ significantly. Most notably, while the inclusion of a substantial contribution from an old component can help reduce the strong NIR features predicted by Ma05 models, the NIR-to-optical ratio predicted by these models remains nevertheless too high.

## 4 SUMMARY AND CONCLUDING REMARKS

We have presented the first spectroscopic study of post-starburst galaxies covering both the optical (SDSS) and NIR (our new VLT-ISAAC observations) wavelength ranges, which was specifically designed to detect the two main signatures of the presence of TP-AGB stars predicted by the Maraston (2005) models in contrast to "TP-AGB light" models (such as BC03): *i)* the strong NIR absorption features caused by carbon composite molecular band-heads; and *ii)* the boosting of the NIR flux. To this goal, we have carefully selected a sample of 16 galaxies with post-burst ages corresponding to the peak contribution by TP-AGB stars to the NIR flux (0.5–1.5 Gyr), in a broad range of stellar metallicities ($\approx$ 0.2–2.5 $Z_{\odot}$). These galaxies are at high enough redshift (0.15–0.25) to allow clean measurements of the NIR features at rest wavelengths 1.41 and 1.77 $\mu$m through the atmospheric H and K windows. Despite these ideal conditions for the detection of the characteristic signatures of TP-AGB stars predicted by the Ma05 models, the 16 galaxies in our sample all display smooth, featureless NIR spectra and blue optical-NIR colours. Interestingly, these observed spectral properties are generally well reproduced using the BC03 models assuming simple (i.e. single-age) stellar populations.

We have investigated whether the observations could be reproduced with Ma05 models as well, by combining stellar populations of different ages. We find that diluting the light of a young (i.e. a few 100 Myr old) starburst with that of a massive old component allows the Ma05 models to reproduce the typical "E+A" optical spectra of post-starburst galaxies characterised by strong Balmer absorption lines and a

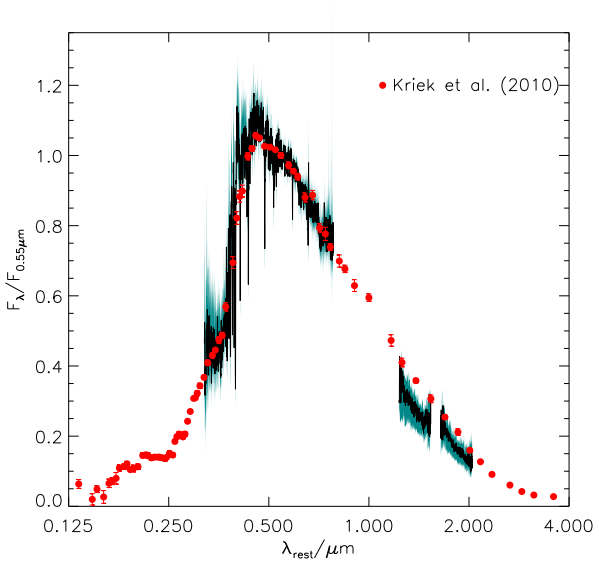


**Figure 11.** Comparison between the stacked SED from our spectra and from the post-starburst sample from the NMBS of Kriek et al.(2010), shown as red points with error bars. The black line is the median spectrum of our 16 galaxies, whose spectra had been previously normalised at 5500 Å. The shaded area shows the 16–84 percentile range of the data. The two samples yield consistent results (although our sample appears marginally biased towards bluer SEDs relative to Kriek et al. 2010) and, most importantly, agree on the fact that there is no need for boosted NIR emission by TP-AGB as implied by Ma05.

well developed D4000 break. At the same time, such models exhibit very weak NIR features, in agreement with the observations, because TP-AGB stars from the young component have not developed yet, while the NIR emission from old stellar populations is smoother. However, these models still cannot account for the data, because the predicted ratio of NIR to optical flux is significantly larger than observed at the metallicity of our galaxies. Hence, the observed lack of deep NIR absorption features and the modest ratio of NIR to optical flux in our data cannot be simultaneously accounted for by a simple "light dilution" effect. We note that the observation of metal absorption lines at optical wavelength does not support the idea that the faint NIR continuum (and the consequent dilution and/or absence of strong NIR absorption features) could arise from extremely low metallicities.

The Ma05 models predict too red optical-NIR colours for any choice of ratio between the old and the young component. On the contrary, models based on BC03 fail for "old" mass fractions as high as 90%, but produce colours that are consistent with (most of) the observations for "old" mass fractions up to 60–70%, which leaves enough space to accommodate more reasonable SFHs than a (possibly unrealistic) single burst. We note that the work of Pracy et al. (2012) indicates old fractions close to 90% for their seven PSB galaxies, which would be inconsistent with our SEDs. However, this estimate might be biased by their assumption of fixed solar metallicity. Moreover, and probably more importantly, it is possible that our objects are somehow more extreme in terms of burst fraction, because, due to our redshift constraints, we select objects close to the faintest limit of the spectroscopic sample of the SDSS. In this way we would select the intrinsically most luminous PSB galaxies at $z \approx 0.2$, hence those with the largest burst fraction (i.e. with the lowest "old" fraction): in fact, for a given total mass, a higher burst fraction yields higher luminosity. The lack of strong colour gradients in most of our PSB galaxies lends support to this hypothesis, suggesting that the starburst substantially affected the full extent of the galaxy, rather than the centre only. Finally, Pracy et al. (2012) point out that their sample is less extreme than typical samples of PSB galaxies in the literature due to the small physical size of the spectroscopic fiber (few hundred parsecs), which bias their selection towards central rather than extended starbursts. In conclusion, the consistency of our SEDs with BC03-based CSPs and "old" mass fractions up to 60–70% does not raise any problem for the physical interpretation of our PSB galaxies using the BC03 models.

We also find that attenuation by interstellar dust, using standard prescriptions, can only worsen the disagreement (when present) between spectral evolution models and the observed optical-NIR colours of post-starburst galaxies in our sample. This is particularly true for the Ma05 models, which predict systematically redder colours than observed. We note that heavier-than-implemented attenuation by *circumstellar* dust of the most luminous C stars about to eject their envelopes could potentially reduce the contribution by these stars to the integrated spectrum and perhaps improve the agreement of the Ma05 models with observations.[14] A more accurate theoretical and empirical assessment of the effects of circumstellar dust absorption is definitely key to make progress in the SED modelling of the stellar population affected by TP-AGB stars (e.g. Srinivasan et al. 2009; Melbourne et al. 2012; Meidt et al. 2012).

The results presented in this work confirm the previous claim by Kriek et al. (2010) that BC03, and more generally "TP-AGB light" models, provide a better agreement with the spectral properties of galaxies hosting a stellar population at the peak of the TP-AGB phase than Ma05 models. The important novelty of our work is to base these conclusions on a higher-resolution, high-quality spectrophotometric dataset and an optimal spectroscopic sample selection.

Somehow in contrast with these studies and our work in particular, Lyubenova et al. (2012) have detected the 1.77 $\mu$m feature in a couple of Magellanic Cloud's globular clusters and found them in agreement with Ma05 predictions. This result calls for more observations in order to obtain a representative sample of globular clusters over a broader range of metallicities (the two in which the detection was obtained are both at metallicity between 0.2 and 0.6 solar) and beat down stochasticity effects: in fact, a single (TP-)AGB star can produce a substantial fraction of the total cluster NIR luminosity in the mass range explored.

[14] The Ma05 models rely on period-averaged spectra of TP-AGB stars assembled by Lançon & Mouhcine (2002), who recommend reddening these spectra before use in population synthesis models (see their section 3.3). Whether this or a different attenuation has been included cannot be asserted from the description of the TP-AGB spectra in section 3.3.2 of Ma05. In the BC03 models, the circumstellar attenuation of TP-AGB stars experiencing superwinds is accounted for in an empirical way (see section 2.2.4 of BC03 for detail).

One further possibility to reduce the apparent disagreement between the Lyubenova et al. (2012) results and ours might reside in a technical aspect of their challenging observations: the addition of targeted AGB stars outside of the central region to integrate the central spectrum and obtain full spatial coverage of the globular clusters might lead to AGB stars being over-represented with respect to the stars that contribute the bulk of the diffuse emission.

In the light of this complex and partly controversial observational framework, the apparent agreement of the BC03 models (of either simple or composite stellar populations) with the observations presented in this paper should not be necessarily interpreted as an indication that the description of the TP-AGB phase in these models is adequate. New models incorporating more recent developments in the theory and observation of TP-AGB stars (e.g. Marigo et al. 2008; Srinivasan et al. 2009; Girardi et al. 2010; Melbourne et al. 2012) are being assembled (Charlot & Bruzual, in preparation). By providing a better account of observations, new models of this type will allow deeper insight into the physical properties of galaxies from spectral interpretations, especially at high redshift, where a large number of galaxies is going through the evolutionary phase affected by TP-AGB stars. In this perspective, the present work provides key and very stringent constraints for the new generation of stellar population synthesis models.

## ACKNOWLEDGMENTS

We thank the anonymous referee for useful comments and suggestions that significantly improved the clarity of the presentation.
The Dark Cosmology Centre is funded by the Danish National Research Foundation.
We also thank Paolo Cassata, Harald Kuntschner and Mariya Lyubenova for useful comments. S.Z. acknowledges the generous hospitality of the Dark Cosmology Centre and stimulating discussions with Jens Hjorth and Sune Toft. D.P. acknowledges the kind hospitality at the Max-Planck-Institut für extraterrestrische Physik.

## REFERENCES

Abazajian K. N., Adelman-McCarthy J. K., Agüeros M. A., Allam S. S., Allende Prieto C., An D., Anderson K. S. J., Anderson S. F., Annis J., Bahcall N. A., et al. 2009, ApJS, 182, 543
Aihara H., et al. 2011, ApJS, 193, 29
Bell E. F., McIntosh D. H., Katz N., Weinberg M. D., 2003, ApJS, 149, 289
Bruzual G., 2007, in Vallenari A., Tantalo R., Portinari L., Moretti A., eds, From Stars to Galaxies: Building the Pieces to Build Up the Universe Vol. 374 of Astronomical Society of the Pacific Conference Series, Stellar Populations: High Spectral Resolution Libraries. Improved TP-AGB Treatment. pp 303–+
Bruzual G., Charlot S., 2003, MNRAS, 344, 1000
Cardelli J. A., Clayton G. C., Mathis J. S., 1989, ApJ, 345, 245
Charlot S., Bruzual A. G., 1991, ApJ, 367, 126
Charlot S., Fall S. M., 2000, ApJ, 539, 718
Chisari N. E., Kelson D. D., 2012, ApJ, 753, 94
Conroy C., Gunn J. E., 2010, ApJ, 712, 833
Conroy C., Gunn J. E., White M., 2009, ApJ, 699, 486
Fukugita M., Ichikawa T., Gunn J. E., Doi M., Shimasaku K., Schneider D. P., 1996, AJ, 111, 1748
Gallazzi A., Charlot S., Brinchmann J., White S. D. M., Tremonti C. A., 2005, MNRAS, 362, 41
Girardi L., Williams B. F., Gilbert K. M., Rosenfield P., Dalcanton J. J., Marigo P., Boyer M. L., Dolphin A., Weisz D. R., Melbourne J., Olsen K. A. G., Seth A. C., Skillman E., 2010, ApJ, 724, 1030
Goto T., 2005, MNRAS, 357, 937
Groenewegen M. A. T., Sloan G. C., Soszyński I., Petersen E. A., 2009, A&A, 506, 1277
Ilbert O., et al. 2010, ApJ, 709, 644
Kannappan S. J., Gawiser E., 2007, ApJ, 657, L5
Korn A. J., Maraston C., Thomas D., 2005, A&A, 438, 685
Kriek M., Labbé I., Conroy C., Whitaker K. E., van Dokkum P. G., Brammer G. B., Franx M., Illingworth G. D., Marchesini D., Muzzin A., Quadri R. F., Rudnick G., 2010, ApJ, 722, L64
Kurucz R. L., 1992, in B. Barbuy & A. Renzini ed., The Stellar Populations of Galaxies Vol. 149 of IAU Symposium, Model Atmospheres for Population Synthesis. p. 225
Lançon A., Mouhcine M., 2002, A&A, 393, 167
Lançon A., Mouhcine M., Fioc M., Silva D., 1999, A&A, 344, L21
Lawrence A., et al. 2007, MNRAS, 379, 1599
Lyubenova M., Kuntschner H., Rejkuba M., Silva D. R., Kissler-Patig M., Tacconi-Garman L. E., Larsen S. S., 2010, A&A, 510, A19
Lyubenova M., Kuntschner H., Rejkuba M., Silva D. R., Kissler-Patig M., Tacconi-Garman L. E., 2012, A&A, 543, A75
MacArthur L. A., McDonald M., Courteau S., Jesús González J., 2010, ApJ, 718, 768
Maraston C., 2005, MNRAS, 362, 799
Maraston C., Daddi E., Renzini A., Cimatti A., Dickinson M., Papovich C., Pasquali A., Pirzkal N., 2006, ApJ, 652, 85
Maraston C., Strömbäck G., 2011, MNRAS, 418, 2785
Marigo P., Girardi L., 2007, A&A, 469, 239
Marigo P., Girardi L., Bressan A., Groenewegen M. A. T., Silva L., Granato G. L., 2008, A&A, 482, 883
Meidt S. E., et al. 2012, ArXiv e-prints
Melbourne J., Williams B. F., Dalcanton J. J., Rosenfield P., Girardi L., Marigo P., Weisz D., Dolphin A., Boyer M. L., Olsen K., Skillman E., Seth A. C., 2012, ApJ, 748, 47
Moorwood A., et al. 1998, The Messenger, 94, 7
O'Donnell J. E., 1994, ApJ, 422, 158
Pracy M. B., Owers M. S., Couch W. J., Kuntschner H., Bekki K., Briggs F., Lah P., Zwaan M., 2012, MNRAS, 420, 2232
Quintero A. D., Hogg D. W., Blanton M. R., Schlegel D. J., Eisenstein D. J., Gunn J. E., Brinkmann J., Fukugita M., Glazebrook K., Goto T., 2004, ApJ, 602, 190
Riffel R., Pastoriza M. G., Rodríguez-Ardila A., Maraston C., 2007, ApJ, 659, L103

Schlegel D. J., Finkbeiner D. P., Davis M., 1998, ApJ, 500, 525
Srinivasan S., et al. 2009, AJ, 137, 4810
Strauss M. A., et al. 2002, AJ, 124, 1810
Thomas D., Maraston C., Bender R., 2003, MNRAS, 339, 897
Thomas D., Maraston C., Bender R., Mendes de Oliveira C., 2005, ApJ, 621, 673
Thomas D., Maraston C., Korn A., 2004, MNRAS, 351, L19
Wright E. L., et al. 2010, AJ, 140, 1868
York D. G., et al. 2000, AJ, 120, 1579
Zibetti S., Charlot S., Rix H., 2009, MNRAS, 400, 1181